Author Manuscript

Author Manuscript

Author Manuscript

Author Manuscript

HHS Public Access

Author manuscript

Mol Cell. Author manuscript; available in PMC 2020 July 11.

Published in final edited form as:

Mol Cell. 2019 July 11; 75(1): 13–25.e5. doi:10.1016/j.molcel.2019.05.004.

Arc oligomerization is regulated by CaMKII phosphorylation of GAG domain; an essential mechanism for plasticity and memory formation.

Wenchi Zhang[1], **Yang-An Chuang**[1], **Youn Na**[1], **Zengyou Ye**[1], **Liuqing Yang**[1], **Raozhou Lin**[1], **Jiechao Zhou**[1], **Jing Wu**[1], **Jessica Qiu**[1], **Alena Savonenko**[4], **Daniel J. Leahy**[3], **Richard Huganir**[1], **David J. Linden**[1], and **Paul F. Worley**[1,2,5,*]

[1]Solomon H. Snyder Department of Neuroscience, Johns Hopkins University School of Medicine, Baltimore, MD 21205, USA

[2]Department of Neurology, Johns Hopkins University School of Medicine, Baltimore, MD 21205, USA

[3]Department of Molecular Biosciences, University of Texas at Austin, Austin, TX 78712

[4]Department of Pathology, Johns Hopkins University School of Medicine, Baltimore, MD 21205, USA

[5]Lead Contact

Summary

Arc is a synaptic protein essential for memory consolidation. Recent studies indicate that Arc originates in evolution from a Ty3/Gypsy retrotransposon GAG domain. The N-lobe of Arc GAG domain acquired a hydrophobic binding pocket in higher vertebrates that is essential for Arc's canonical function to weaken excitatory synapses. Here, we report that Arc GAG also acquired phosphorylation sites that can acutely regulate its synaptic function. CaMKII phosphorylates the N-lobe of Arc GAG domain and disrupts an interaction surface essential for high order oligomerization. In Purkinje neurons CaMKII phosphorylation acutely reverses Arc's synaptic action. Mutant Arc that cannot be phosphorylated by CaMKII enhances metabotropic receptor-dependent depression in the hippocampus but does not alter baseline synaptic transmission or

*Correspondence: pworley@jhmi.edu.

Author Contributions

W.Z. performed biophysical studies. Y.C., Y.N., J.Q. and L.Y. identified and validated phosphorylation sites and run behavioral studies. R.L., J.Z. and J.W. helped with imaging analysis. D.J.L. performed electrophysiological studies in Purkinje neurons. Z.Y. performed hippocampal slice recordings. A.S. analyzed behavioral data. R.L.H, A.S., D.J.L, D.J.L. and P.F.W oversaw experiments, P.F.W wrote manuscript with assistance from co-authors.

Publisher's Disclaimer: This is a PDF file of an unedited manuscript that has been accepted for publication. As a service to our customers we are providing this early version of the manuscript. The manuscript will undergo copyediting, typesetting, and review of the resulting proof before it is published in its final citable form. Please note that during the production process errors may be discovered which could affect the content, and all legal disclaimers that apply to the journal pertain.

Declaration of Interests

The authors declare no competing interests.

Supplemental Information

Document S1. Figures S1–S7

Data and Software Availability

The raw imaging data have been deposited in Mendeley website: http://dx.doi.org/10.17632/tt3hrs3r2m.1

Author Manuscript Author Manuscript Author Manuscript Author Manuscript

long-term potentiation. Behavioral studies indicate that hippocampus- and amygdala-dependent learning require Arc GAG domain phosphorylation. Studies provide an atomic model for dynamic and local control of Arc function underlying synaptic plasticity and memory.

Graphical Abstract

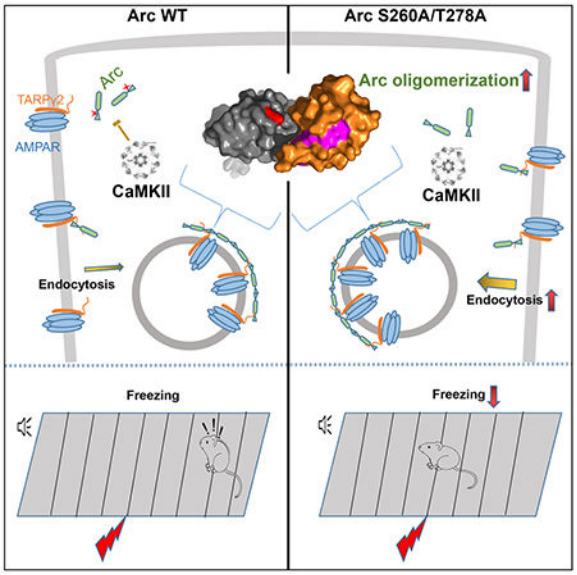

eTOC blurb

Normal learning and memory require dynamic control of synaptic connections. Arc plays a critical role in modifying synaptic strengths. Zhang et al. reveal that Arc's function is controlled by a novel regulatory mechanism that exploits its evolutionary origin as a retrotransposon GAG domain together with CaMKII that records activity history.

Introduction

Classical studies demonstrated that long-term memory requires rapid *de novo* mRNA and protein synthesis (Goelet et al., 1986; Kandel et al., 2014). One of the enduring challenges is how the *de novo* response can target and modify specific synapses that are the basis for information storage. *Arc* (also termed *Arg3.1)* provides an exemplary gene since its mRNA and protein are rapidly induced in response to learning behaviors (Guzowski et al., 1999; McCurry et al., 2010; Moorman et al., 2011) and genetic deletion disrupts long-term but not short-term learning (Plath et al., 2006). To identify post-translational mechanisms that could locally regulate Arc protein function, we performed a mass spectrometric analysis following immune isolation from mouse brain. We identified two phosphorylation sites and confirmed that one site, ArcS260, is dynamically phosphorylated by CaMKII. Arc binds CAMKII (Okuno et al., 2012; Zhang et al., 2015), and Arc's preferential association with inactive CaMKIIß appears to contribute to Arc localization to inactive synapses (Okuno et al., 2012). However, a role of CaMKII kinase activity in control of Arc function was previously unknown.

Author Manuscript Author Manuscript Author Manuscript Author Manuscript

ArcS260 lies within a structural domain of Arc, termed the Arc GAG domain, which we recently resolved by crystallography (Zhang et al., 2015). Like retroviral GAG domains, Arc GAG includes a contiguous N-lobe and C-lobe. In higher vertebrates Arc N-lobe acquired a hydrophobic binding pocket that is required for Arc to bind CaMKIIα and CaMKIIβ, as well and other synaptic proteins including TARPγ2/4/8, GKAP, GluN2A/B, and WAVE1, and is required for the action of Arc to weaken synapses (Zhang et al., 2015). ArcS260 is remote from the binding pocket but close to inter-protomer contact surfaces of the N-lobe crystal structure. Similar surfaces in HIV GAG domain mediate viral capsid assembly (Pornillos et al., 2009; Pornillos et al., 2011). Structure-function analysis reported here demonstrates an essential role for inter-protomer interactions of both N-lobe and C-lobe for high order oligomerization of full-length Arc and further demonstrates that these interaction surfaces are required for Arc's synaptic function. Arc point mutants that mimic CaMKII phosphorylation can bind synaptic proteins and endocytic vesicles but fail to form high order oligomers and lack the ability to weaken synapses. We generated a mouse genetic model expressing mutant Arc that cannot be phosphorylated by CaMKII and found that baseline synaptic transmission and LTP in the hippocampus appear normal but metabotropic receptor-LTD is increased in magnitude. This finding suggests that the efficacy of mGluR-LTD is normally controlled by local CaMKII activity. Behavioral studies indicate that Arc GAG domain phosphorylation is essential for normal learning. The present findings reveal an essential regulatory mechanism for the function of Arc that couples its action to the local activity history of synapses.

Results

Arc GAG domain is dynamically phosphorylated by CaMKII.

We performed a Mass Spectrometric (MS) analysis of Arc immunoprecipitated from detergent lysates of naïve adult wild-type (WT) mouse forebrain (Figure 1A and 1B), and identified multiple peptides of Arc including 2 potential phosphorylation sites within the Arc GAG domain (Figure 1C and S1A). Phosphorylation sites were identified in two independent experiments. Amino acid coverage was ~90% over the Arc GAG domain (a.a. 201-360). ArcS260 is a predicted site for CaMKII or PKC α/β/γ/δ/ζ and ArcT278 is a predicted PKC δ/ε site (https://scansite4.mit.edu).

We generated phosphospecific antibodies (Abs) that reacted with Arc transgene immunoprecipitated from HEK293 cells co-transfected with activated CaMKIIα but not ArcS260A (Figure 1E). Arc immunoprecipitated from mouse forebrain reacted with phospho ArcS260 Ab and this was abolished by lambda protein phosphatase (Figure 1F). Arc pS260 immunoreactivity was induced in cultured cortical neurons upon addition of bicuculline to increase excitatory activity and was blocked by CaMKII inhibitor KN93 but not the inactive compound KN92 (Figure 1G). CaMKII is activated in response to bicuculline treatment of primary neuronal cultures (Shin et al., 2012). The pharmacology and predicted consensus indicate that Arc S260 is phosphorylated by CaMKII.

Antisera generated against phospho ArcT278 peptide reacted with Arc transgene from HEK293 cells treated with PKC activator, phorbol 12 13-diacetate (PDA). Both the basal and PDA stimulated signal were absent for ArcT278A (Figure S1B). However, phospho

Author Manuscript Author Manuscript Author Manuscript Author Manuscript

ArcT278 Ab did not react with Arc immunoprecipitated from brain or cultured neurons treated with the PKC activator phorbol-12,13-diacetate (PDA; data not shown). We conclude that Arc can be phosphorylated at both S260 and T278, but in current conditions only ArcS260 is validated in neurons.

Structural basis of Arc oligomerization.

Arc N-lobe (a.a. 207-278) and C-lobe (a.a. 278-370), which together form the Arc GAG, are each composed of four alpha helices surrounding a hydrophobic core (Zhang et al., 2015). Arc N-lobe helix α4 is contiguous with Arc C-lobe helix α1', and these are separated by a putative hinge region. Hydrophobic amino acids that form the core of Arc N-lobe in lower-vertebrates are replaced in higher vertebrates creating a pocket that accommodates aromatic side chains of bound ligands including TARPγ2 and CaMKII (Zhang et al., 2015). The positions of phosphorylation sites ArcS260 and ArcT278 can be visualized in the structure of Arc N-lobe in complex with either TARPγ2 or CaMKII (Figure 2A, 2B and S7). ArcS260 is at the C-terminus of helix α3 while ArcT278 is at the putative hinge region between the lobes. Both phosphorylation sites are distant from the Arc N-lobe hydrophobic pocket and bound ligand, but close to surfaces between adjacent N-lobe protomers in the crystals (Figure 2A and 2B). Accordingly, we considered the possibility that inter-protomer interactions identified from the crystal structure might be physiologically relevant and modified by phosphorylation. We noted that Arc N-lobe interaction surfaces are identical in two independent complex structures that display different symmetry groups, are similar to Arc C-lobe (Figure 2C), and are similar to HIV C-lobe interactions important for retrovirus capsid assembly (Figure 2D) (Pornillos et al., 2009; Pornillos et al., 2011). The combined buried area of N-lobe and C-lobe putative interaction surfaces is greater than 960 $Å^2$ and comparable to the combined areas of retroviral capsids (Pornillos et al., 2009; Pornillos et al., 2011). Moreover, the degree of "fit" of interaction surfaces assessed by a calculated shape correlation (SC) (Lawrence and Colman, 1993) (SC of 1 indicates precise meshing while 0 indicates uncorrelated topography) is 0.717 for Arc N-lobe and 0.697 for Arc C-lobe. These SCs are comparable to physiologically relevant interaction surfaces (Rouvinski et al., 2015). Surfaces that mediate inter-protomer associations of the rat Arc N-lobe and C-lobe are evolutionarily conserved (Figures 3A and 4A).

We monitored oligomerization using dynamic light scattering (DLS) in various conditions of incubation temperature and protein concentration. As reported (Byers et al., 2015; Myrum et al., 2015; Pastuzyn et al., 2018), full-length bacterially expressed Arc protein (isolated at 4°C) oligomerizes in solution (Figure 3D) and is temperature dependent. HIV GAG shows similar temperature-dependent oligomerization (Barklis et al., 2009) that is relevant to viral capsid assembly (Serriere et al., 2013). At 20°C, a 10 μM solution of Arc had a calculated mass of 210 kDa indicating Arc behaves as a stable tetramer. Arc tetramer formation is dependent on the N-terminal half of Arc that includes basic, α-helical regions thought to associate with phospholipid membranes (Myrum et al., 2015) since isolated Arc GAG domain remains monomeric at 20°C or 30°C even at 200μM (Figure S2A). Upon shifting the solution to higher temperature and maintaining for an additional 20 min, full-length Arc exhibited an increase in estimated radius indicating higher order oligomerization. Higher incubation temperature (up to 37°C) or higher initial concentration of full-length Arc

Author Manuscript Author Manuscript Author Manuscript Author Manuscript

resulted larger oligomers. In all conditions a single peak of oligomeric state was observed, confirming that the protein solution was homogeneous and not irregular misfolded aggregates (Figure 3D and S2B). During incubation, the mean molecular weight species increased steadily in solution without stabilized plateau (Figure S2B). Oligomerization at 30°C was reversible upon return to 20°C until the average molecular weight reached ~800 kDa (an tetramer of Arc tetramers) (Figure S2C), which supports the notion that oligomers assemble in a reversible, temperature-dependent process. Based on these results, experiments were performed at 30°C with an initial protein concentration of 0.5 mg/ml in the remainder of the study, where the estimated radius of the 12 nm peak corresponds to ~1860 kDa (an octomer of Arc tetramers) at the end of a 20 min incubation period.

Next, we examined the N-lobe structure to identify specific amino acids that mediate inter-protomer interactions and test their effect on oligomerization of full-length recombinant Arc. Intermolecular associations of Arc N-lobe mediated by the first two α-helices of monomer A packed against the last two α-helices of monomer B buries areas of 421 $Å^2$ per protomer (Figure 3B). The aromatic side-chain of F256 at the center of the bundle forms a small hydrophobic core, whereas polar residues at the periphery participate in hydrophilic interactions. Hydrogen bond interactions, predicted based on distances < 4 Å, occur between side chains of contiguous monomers K257-Q241, K257-N244 and W253-Y237 (Figure 3B). K257 also bonds with E270 of the same monomer and is within 4.6 Å of S260 (Figure 3C). Analysis of charge proximity suggests an important role for the long flexible basic side chain of K257 that can function as a bridge between monomers. Consistent with this analysis full-length Arc mutants ArcK257A and ArcQ241A formed tetramers at 20°C but failed to oligomerize at 30°C (Figure 3D).

Arc C-lobe protomers associate in the crystal structure by interactions between α2 of protomer A and α3 of protomer B and exhibit the same symmetry as Arc N-lobe homophilic interactions (Figure 2C). The Arc C-lobe buried surface area 546$Å^2$ compares to 922$Å^2$ of HIV C-lobe interface and 612$Å^2$ of RSV C-lobe interface. Like Arc N-lobe, basic amino acid side chains form a bridge between C-lobe protomers. Arc R335 (monomer B) hydrogen bonds with E320 (monomer A) while R338 and H339 (monomer A) hydrogen bond with D289 and Y313 (monomer B)(Figure 4B). Point mutants of all of these sites were generated but only Arc R335E expressed. DLS demonstrated ArcR335E behaves like WT at 20°C but fails to oligomerize at 30°C (Figure 4C). These findings indicate that interactions mediated by both the Arc N-lobe and Arc C-lobe are required for high order oligomerization of full-length Arc.

The interaction surfaces for both Arc N-lobe and C-lobe that mediate oligomer assembly are asymmetric in that they involve different surfaces of protomer A and protomer B (Figure 2A, 2B, and 2C). This creates flexibility for oligomer assembly with four different possible configurations of each full-length Arc molecule within an oligomer (Figure S2D and S2E) and may underlie the variable size of Arc oligomers. This is distinct from retroviral capsid assembly, which is largely mediated by symmetric interactions between lobes (Figure 2D) and creates oligomers of fixed size (Serriere et al., 2013).

Author Manuscript Author Manuscript Author Manuscript Author Manuscript

Phosphomimic mutations of Arc disrupt high order oligomerization

We examined a panel of full-length Arc point mutants to assess the effect of negative charge at phosphorylation sites. Phosphomimetic mutants ArcS260D, ArcS260D,T278D and ArcS260D,T278A formed tetramers at 20°C but did not oligomerize at 30°C (Figure 3E). By contrast, ArcS260A,T278A and ArcS260A displayed temperature-dependent oligomerization. ArcS260 is 4.61Å from the basic residue of K257 (Figure 3C) and the added volume of S260 phosphate will reduce the distance to K257 for salt bridge formation. These observations indicate that addition of negative charge at ArcS260 prevents temperature-dependent oligomerization and supports a model in which phosphorylation of S260 promotes an intramolecular salt bridge with nearby K257 that competes with intermolecular interactions needed for high order oligomerization.

ArcT278D formed tetramers at 20°C and high order oligomers at 30°C although the size was less than WT Arc (Figure 4D). ArcT278 is within an extended alpha helical region that spans Arc N-lobe α4 to the Arc C-lobe α1' (Figure 3A and Figure 4A) but is not sufficiently constrained to be resolved in either crystal structure. Contiguous G277 is predicted to confer flexibility between Arc N- and C-lobes. The demonstrated importance of flexibility between retroviral GAG N-lobe and C-lobe domains for capsid assembly (Pornillos et al., 2009; Pornillos et al., 2011) suggested that flexibility at ArcG277 may be important for oligomerization. Consistent with this model, ArcG277D formed tetramers at 20°C but failed to form high order oligomers at 30°C (Figure 4D). The proximity of ArcT278 to the putative hinge suggests that if phosphorylation of ArcT278 occurs *in vivo* it may inhibit or slow oligomerization by reducing necessary flexibility between lobes.

Interaction surfaces essential for high order oligomerization of Arc are required for its function to depress synaptic strength.

We compared the structure-function relationship for Arc oligomerization and synaptic depression in Purkinje neurons. Parallel fiber inputs to Purkinje neurons exhibit activity-dependent depression that is induced by postsynaptic activation of metabotropic glutamate receptors (mGluR-LTD)(Linden, 2012). Arc is expressed at low basal levels in Purkinje cells and does not contribute to the early phase of LTD but is transcriptionally induced and is required for the protein synthesis-dependent late phase of LTD (Smith-Hicks et al., 2010). Consistent with these studies, whole-cell voltage-clamp recordings made from mouse Purkinje cells expressing WT Arc transgene in cultures revealed reduced miniature excitatory post-synaptic current (mEPSC) amplitudes (Figure 5A). Moreover, Arc transgene expression occluded chemical LTD evoked by treatment of neurons with PDA (Figure 5A). The CaMKII inhibitor KN-93 did not alter effects of Arc on baseline synaptic strength or occlusion of PDA (Figure 5A).

We next examined Arc point mutants in Purkinje neurons. Mutant Arc proteins that do not form high order oligomers including ArcS260D, ArcS260D/T278D and ArcR335E lacked WT Arc function and did not reduce the amplitude of mEPSCs or occlude PDA-induced LTD (Figure 5B). By contrast, mutant Arc proteins that do form high order oligomers including ArcS260A, ArcS260A/T278A and ArcT278D behaved like WT Arc to reduce the amplitude of spontaneous mEPSCs and occlude the effect of PDA treatment (Figure 5B). As

Author Manuscript Author Manuscript Author Manuscript Author Manuscript

controls for these studies we confirmed that mutations of Arc that disrupt high order oligomerization do not disrupt binding of full-length Arc to TARPγ2 peptide (Figure S3A). Additionally, we examined the subcellular localization of WT and mutant Arc transgenes in neurons co-transfected with the interacting vesicle protein endophilin3 as well as GFP-Rab5, GFP-Rab7 and GFP-Rab11 to mark specific vesicle populations. WT Arc, ArcS260D/T2278D and ArcS260A/T2278A showed similar co-IP with endophilin3 transgene from HEK293 cells (not shown), and co-localization in neuronal dendrites on punctate structures (presumed endosomes) with endophilin3, Rab5, Rab7 and Rab11 transgenes (Figure S3B–D). Thus, mutations that inactivate Arc synaptic function do not necessarily prevent its association with vesicles. These findings are consistent with a model in which the N-terminal half of Arc contributes importantly to oligomerization, mediates association with endophilin and dynamin (Chowdhury et al., 2006), is basic and palmitoylated to enhance association with phospholipids (Barylko et al., 2018; Myrum et al., 2015), but individual interactions of N-lobe and C-lobe are required for high order oligomerization and Arc's canonical synaptic function.

Input-specific reversal of Arc by CaMKII activation.

To examine input-specific effects of Arc we examined the late phase of cerebellar LTD using a well-established protocol in which two iontophoresis electrodes are positioned to stimulate separate dendritic branches of cultured Purkinje neurons in an alternating fashion. Following acquisition of baseline responses to test pulses of glutamate, test pulses are halted at the "control" electrode and LTD is induced by applying glutamate/depolarization conjunctive stimulation at the "paired" electrode. This results in input-specific induction of LTD (Linden, 2012; Wang and Linden, 2000). In Purkinje neurons expressing Arc transgene glutamate/depolarization conjunctive stimulation at the "paired" electrode at t= 0 min resulted in an unexpected, rapid potentiation of the "control" pathway (Figure 5C). Potentiation was evident within 5 min and subsequent bouts of conjunctive stimulation at 1= 10 and 20 min evoked a saturating potentiation that persisted to the end of the recording at t=90 min. We termed this phenomenon Arc-dependent heterosynaptic LTP (Arc-hLTP). Arc-hLTP required both glutamate stimulation of the paired pathway and somatic depolarization since either manipulation alone failed to evoke potentiation of the control pathway (not shown).

Combined depolarization and glutamate stimulation results in a cell-wide rise of Ca^{2+} (Linden, 2012), and we considered the possibility that this stimulus activates CaMKII and acutely reverses the synaptic action of Arc. Consistent with this mechanism, bath application of the CaMKII inhibitor KN93 (5 μM) prevented Arc-hLTP without changing the amplitude of the response in the paired pathway (Figure 5C). We noted that activation of PKC by PDA did not result in reversal of Arc action (Figure 5A) and experiments monitored the effect of the PI3Kinase inhibitor Wortmannin (1 μM) and found no effect on Arc-hLTP (not shown). We repeated the experiment in Purkinje neurons expressing ArcS260A or ArcS260A/T278A. Purkinje neurons expressing either mutant failed to show Arc-hLTP of the control pathway (Figure 5D). These observations support the model that CaMKII oligomerization-disrupting phosphorylation of ArcS260 acutely reverses Arc's synaptic weakening function in Purkinje neurons.

Author Manuscript Author Manuscript Author Manuscript Author Manuscript

Arc phosphorylation controls the magnitude of mGluR-LTD at the Schaffer collateral-CA1 synapse.

To examine the role of Arc GAG domain phosphorylation in neural plasticity *in vivo*, we generated a knock-in murine model (Figure S4). $Arc^{S260A/T278A}$ KI mice were backcrossed at least five generations to C57BL/6J. Homozygous $Arc^{S260A/T278A}$ KI mice (Arc 260/278 AA/AA) are viable, produce offspring according to Mendelian genetics, show normal brain morphology, and reach the same body weight at adulthood as wild-type littermates. The basal expression of Arc protein and mRNA transcript in Arc 260/278 AA/AA was comparable to WT mice, and there was no significant difference in the expression of PSD95, TARPγ2, NMDAR subunits, AMPAR subunits, or mGluR subunits (Figure S4).

Electrophysiological recordings of the Schaffer-CA1 synapse were performed using acute hippocampal slices and field recordings. Recordings of the baseline relationship between the presynaptic fiber volley amplitude and the slope of the evoked postsynaptic potential revealed similar synaptic strength (Figure 6A). An assessment of the paired pulse ratio suggests similar presynaptic release probability (Figure 6B). We next examined theta burst induced LTP and found that it was not different comparing WT and Arc 260/278 AA/AA slices (Figure 6C). By contrast, mGluR-LTD evoked by bath application of (S)-3,5-dihydroxyphenylglycine (DHPG) revealed enhanced magnitude of depression in Arc 260/278 AA/AA slices (Figure 6D). The maximum stable synaptic depression in WT slices was 18% 20 min after induction and 30% 20 min after induction in Arc 260/278 AA/AA slices. We considered the possibility that Arc protein induced by DHPG might impact subsequent TBS induced LTP, however, when the baseline was adjusted to compensate for enhanced mGluR-LTD in Arc 260/278 AA/AA slices there was no difference compared to LTP in WT slices (Figure 6D and S5). We conclude that genetic interruption of Arc GAG domain phosphorylation has the effect of selectively increasing the magnitude of mGluR-LTD.

Phosphorylation of Arc GAG domain is essential for learning and memory.

Arc 260/278 AA/AA and littermate WT mice were trained in a delayed fear conditioning paradigm, in which presentation of an auditory cue (conditioned stimulus, CS) in a training context was repeatedly paired with an intrinsically aversive stimulus (mild footshock, US). Arc 260/278 AA/AA mice showed deficits in acquisition of fear to context as judged by development of freezing response during intertrial intervals (Figure 7A–B). The learning deficit in Arc 260/278 AA/AA mice was also observed as a low acquisition of freezing to CS (Figure 7C). This learning deficit could not be explained by changes in sensitivity to the US as both genotypes demonstrated comparable levels of motor activation and body displacement by the footshock (Figure 7A insert). The role of anxiety as a non-cognitive factor in this deficit was also unlikely as Arc 260/278 AA/AA mice were not different from controls avoiding anxiogenic areas in plus maze and open field (Figure S6). Testing for long-term contextual memory revealed that Arc 260/278 AA/AA mice demonstrated significantly lower levels of freezing responses than their WT littermates (Figure 7D–E and 7G). Similarly, long-term memory of the CS when tested in a new context was significantly impaired in Arc 260/278 AA/AA mice (Figure 7F and 7H–I). The new context did not support generalization of fear from the previous context (Figure 7G) allowing for testing the

Author Manuscript Author Manuscript Author Manuscript Author Manuscript

acquisition of second-order conditioning (Gewirtz and Davis, 2000; Helmstetter and Fanselow, 1989; Rizley and Rescorla, 1972). This phenomenon represents the association of the CS with a new context resulting in acquirement of freezing responses to the context that was not associated with the US. Presentation of the CS in the new context increased freezing to this context in WT mice (Figure 7F and 7J). However, Arc 260/278 AA/AA mice did not show consistent freezing responses in this situation (Figure 7F and 7J). As second-order conditioning is supported by strong US-CS associations (Helmstetter and Fanselow, 1989), the deficits of Arc 260/278 AA/AA mice acquiring second-order freezing response might be a result of their primary deficits in the first-order conditioning. Similarly, the impairments observed in Arc 260/278 AA/AA mice in long-term fear memory are likely consequences of their principal deficits in ability to quickly acquire the conditional associations during learning phases. Testing of Arc 260/278 AA/AA mice in the Morris water maze that requires many more trials than classical fear conditioning revealed only marginal deficits in spatial memory (Figure S6). Thus, Arc 260/278 AA/AA genetic perturbation is sufficient to deteriorate fast acquisition of new memories. This effect was observed for acquisition of hippocampus-dependent contextual memories as well as for acquisition of amygdala-dependent cued memory (Phillips and LeDoux, 1992) indicating that the functional role of CaMKII-dependent phosphorylation of Arc is not limited to hippocampus-specific neuronal circuit.

Evolution of Arc and regulation by phosphorylation

Surfaces that can mediate asymmetric homophilic interactions between Arc N-lobe and Arc C-lobe proteins are conserved in all species (Figures 3A and 4A). Nevertheless, Arc N-lobe has undergone marked evolutionary changes consistent with the observation that N-lobes of GAG domains evolve for distinct functions (Campillos et al., 2006; Volff, 2009; Zhang et al., 2015) while C-lobes maintain conserved functions. Arc N-lobe from *Drosophila* lacks both the hydrophobic pocket and regulatory phosphorylation sites important for synaptic function in higher vertebrates. Arc N-lobe in *Xenopus* lacks α1 elements essential for a binding pocket (Zhang et al., 2015) and lacks the phosphorylation sites identified here that can regulate oligomerization (Figure 3A). Arc N-lobes of vertebrates from reptile *Anolis carolinensis* to humans possess a conserved hydrophobic binding pocket, predicted phosphorylation sites at S260 and T278, and glycine hinge at 277.

Discussion

The present study reveals the atomic basis of Arc GAG domain’s contribution to high order oligomerization, its regulation by CaMKII, and the evolutionary origin of the regulatory mechanism. High order Arc oligomerization requires asymmetric homophilic interactions of both the Arc N-lobe and Arc C-lobe. This mode of assembly is distinct from retroviral capsid assembly that is based largely on symmetric interactions between lobes (Pornillos et al., 2009; Pornillos et al., 2011) and likely underlies the flexibility of Arc oligomer size. Arc N-lobe homophilic interactions are disrupted by phosphorylation of ArcS260 and all available data indicate that CaMKII phosphorylates ArcS260. In Purkinje neurons, activation of CaMKII acutely reverses the function of Arc to weaken synapses and results in heterosynaptic LTP. Arc binds CaMKII independently of kinase-substrate interaction at a

Author Manuscript Author Manuscript Author Manuscript Author Manuscript

site immediately C-terminal to the CaM binding site that is highly conserved in CaMKIIα and CaMKIIß (Zhang et al., 2015 and Figure S7). This site appears accessible for Arc binding in the cryoEM structure of the inactive enzyme (Myers et al., 2017). Arc-CaMKII binding is unusual for kinase-substrate pairs and is likely important to position Arc to be especially sensitive to CaMKII activity (see below). The role of a second, putative PKC phosphorylation site, ArcT278, at the hinge domain between Arc N-lobe and Arc C-lobe remains unknown. Capacity for high order oligomerization appears not to be essential for Arc to associate with endophilin on endosomes and is not essential for binding TARPγ2 in biochemical assays using GST tethered Arc. High order oligomerization of Arc likely occurs shortly after *de novo* translation in neuronal dendrites and may be necessary to achieve sufficient avidity for Arc to function as a flexible physical scaffold since Arc N-lobe binding affinities for several ligands including TARPγ2 are relatively low [in the range of 10-60 uM (Zhang et al., 2015)].

Observations support the notion that local signaling that controls CaMKII activity regulates Arc function and is required for normal synaptic plasticity. Previous studies have suggested that newly synthesized Arc protein moves from sites of regulated translation within dendritic segments (Na et al., 2016) to synapses where it accumulates based on its binding to CaMKIIß in its inactive state (Okuno et al., 2012). This mechanism may contribute to trafficking, but differential synaptic action based upon Arc-inactive-CaMKIIß binding requires that a substantial percentage of CaMKIIß be activated in order to influence Arc's distribution. This model is challenged by the observation that in physiological conditions only a small fraction of total CaMKII is activated (Feng et al., 2011; Lisman and Raghavachari, 2015; Otmakhov et al., 2015). The present study supports a model in which Arc-CaMKII binding is important to bring the substrate (Arc) in dynamic association with CaMKII, and it is CaMKII kinase activity that is the critical determinant that regulates (inhibits) Arc's synaptic action. In this model, Arc oligomerization and synaptic action can be finely tuned in accordance with the elegant mechanisms that regulate CaMKII activity at individual synapses (Hell, 2014; Lisman and Raghavachari, 2015).

CaMKII is most widely studied for its role in synaptic potentiation (Hell, 2014; Lisman and Raghavachari, 2015). But LTP of the Schaffer-CA1 synapse was not different in Arc 260/278 AA/AA mice than WT littermates. We infer that mechanisms other than CaMKII inhibition of Arc prevent the action of Arc at potentiated synapses, and note that CaMKII phosphorylates TARPγ2/8 at the Arc binding site preventing Arc N-lobe binding (Tomita et al., 2005; Zhang et al., 2015), while reciprocally enhancing PSD95 binding and trafficking of TARPγ2/8-AMPAR to synapses (Sumioka et al., 2010). In contrast, phosphorylation of Arc appears to regulate the magnitude of mGluR-LTD in the hippocampus. Arc is required for mGluR-LTD (Park et al., 2008; Waung et al., 2008) and mGluR-LTD is enhanced by manipulations that up-regulate Arc expression including FMRP KO (Niere et al., 2012), priming (Jakkamsetti et al., 2013), or mutation of Arc to disrupt ubiquitination (Wall et al., 2018). Accordingly, interruption of CaMKII phosphorylation of Arc results in a gain-of-function phenotype indicating that CaMKII normally acts to limit Arc-dependent synaptic weakening. A previous study reported that CaMKII inhibitor increases the magnitude of mGluR-LTD in the hippocampus (Schnabel et al., 1999) and CaMKII is activated during the process of scaling in response to increased activity (Shin et al., 2012). Just as CaMKII

Author Manuscript Author Manuscript Author Manuscript Author Manuscript

activity bound to NMDA receptors “records” the activity history of potentiated synapses (Lisman and Raghavachari, 2015) it is possible that CaMKII activity at non-potentiated synapses records the history of activity relevant for future mGluR-LTD. This mechanism and its potential to regulate the amplitude of mGluR-LTD at individual synapses appears critical for learning and anticipates contributions of Arc and CaMKII to heterosynaptic plasticity attributed to Arc in the visual cortex (El-Boustani et al., 2018) and forms of metaplasticity (Cooper and Bear, 2012).

The retroviral origin of Arc bequeaths unique properties that are exploited by host organisms in an evolutionary process termed “domestication” (Campillos et al., 2006). Recent studies indicate a remarkable new function for Arc that is dependent on its GAG domain. *Drosophila* Arc (dArc1) protein acts like a retroviral particle binding to *dArcl* mRNA and trafficking the mRNA across the synapse to muscle in a process that is essential for normal development of the neuromuscular junction (Ashley et al., 2018). A similar mode of trans-cellular transfer of *Arc* mRNA has been reported for mammalian Arc and requires high order oligomerization mediated in part by Arc C-lobe (Pastuzyn et al., 2018). To the extent that trans-cellular actions Arc are dependent on high order oligomerization, the present study provides a mechanism for regulatory control by synaptic activity history and CaMKII.

STAR Methods

Contact for Reagent and Resource Sharing

Further information and requests for resources and reagents should be directed to and will be fulfilled by Paul Worley (pworley@jhmi.edu).

Method Details

Expression constructs and antibodies—All the expression constructs were made by PCR and cloned into expression vectors pGEX-6P-1 or pRK5. Point mutants were made using Quick Change Site-Directed Mutagenesis Kit (Stratagene). The sequence of the primers used to generate each mutant will be supplied upon request. All constructs were verified by DNA sequencing.

Rabbit polyclonal phosphospecific antibodies for ArcS260 and ArcT278 were generated and affinity purified by AnaSpec Inc. using Arc pS260-EFKQG{pSER}VKNW, Arc pT278-QYSEG{pTHR}LSRE.

Protein expression and purification—cDNAs of full-length Rn Arc (GenBank ID NP_062234) and Arc GAG domain (residues 207-370) were subcloned into vector pGEX-6P-1 (GE Healthcare) between the EcoRI and XhoI restriction sites for bacterial expression as a GST-fusion protein. The transfected E. coli Rosetta (DE3) cell culture was grown at 37°C until OD600 nm reached 0.6. The temperature was reduced to 25°C, and cells were induced with 0.2 mM isopropyl-β-D-thiogalactopyranoside (IPTG) and grown for 16 h. The cells were harvested and lysed by sonicating in PBS (phosphate buffered saline, pH 7.3) supplemented with 1% Triton X-100. The recombinant protein in the supernatant of the cell lysate was mixed with Glutathione Sepharose resin (GE Healthcare) and the mixture was washed extensively in PBS with 1% Triton X-100. After cleaving with Precision protease

Author Manuscript Author Manuscript Author Manuscript Author Manuscript

overnight to remove the GST tag the protein was purified by using Q Sepharose Fast Flow and Superdex 75 size-exclusion chromatography, and was exchanged into a buffer of 20 mM Tris-HCl (pH 8.0), 100 mM NaCl and 1 mM DTT (dithiothreitol) and concentrated to 5 mg/ml.

The cDNA of mouse TARPγ2 (GenBank ID NP_031609) cytoplasmic region (residues 203-323) was subcloned into vector pGEX-6P-1 (GE Healthcare) between the EcoRI and XhoI restriction sites for expression in E. coli. Recombinant proteins contained an N-terminal GST-tag and were purified with GSH-affinity chromatography and further by SP Sepharose Fast Flow after removing the GST tag.

Dynamic light scattering—Purified WT full-length Arc protein or Arc mutant proteins in PBS pH 7.4 with 1mM DTT and 1mM EDTA were concentrated to 0.5 mg/ml. DLS experiments were conducted using a dynamic light scattering instrument DynaPro (Wyatt Technology) controlled by Dynamics™ v.6 software. Samples were equilibrated at starting temperature 20 °C for approximately 10 min. Arc polymerization was triggered by increasing the incubation temperature 1°C every minute to 30°C, then was monitored for an additional 20 minutes at 30°C. DLS measures were collected every 2 min. Each measure was the mean of 15 runs and there were at least two replicates for WT Arc and each mutant.

GST pull-down assay—*E. coli* expressed GST fusion protein that is immobilized on glutathione-Sepharose beads was used to incubate with *E. coli* expressed protein at 4°C for 4 hr. After incubation, glutathione-Sepharose beads were washed with 0.5~1.0% Triton X-100 buffer (in PBS) 3 times. Elutes from beads were used for SDS-PAGE gel electrophoresis and Coomassie blue staining.

Hippocampal and HEK293T cell culture and Transfection—All animal procedures were approved by Johns Hopkins University Animal Care and Use Committee. Mouse cortical cultures from E16.5-E17.5 mouse pups were prepared as reported previously (Rumbaugh et al., 2003). Neurons were fed twice per week with glial-conditioned neurobasal medium and kept at 37°C in 5% CO_2 for 14–18 days in vitro (DIV). HEK293T cells were maintained in Dulbecco's modified Eagle's medium (DMEM) with 10% fetal bovine serum. Transfection was performed with FuGENE6 by manufacturer's instruction (Roche).

Immunoprecipitation Assay—Mouse brain lysates or high-density mouse cortical cultures were harvested in RIPA buffer with protease/phosphatase inhibitors. The lysates were sonicated 3 times for 1 second each, and centrifuged at 13,000rpm for 20 minutes. Supernatant was then mixed with mouse Arc monoclonal antibody (Zhang et al., 2015) for 4 −16 hrs at 4 °C and Protein G Sepharose (Amersham-Pharmacia Biotech) was added for an additional 2 hr. Beads were washed three times with RIPA buffer, eluded with SDS sampling buffer, and analyzed by SDS-PAGE and western blotting.

Mass spectroscopy—Immunoprecipitated Arc protein was excised from SDS-PAGE and processed for MS by digestion with Chymotrypsin or Trypsin. MS was performed at the Taplin Facility at Harvard. The total tryptic peptide pool was directly analyzed by matrix-

Author Manuscript Author Manuscript Author Manuscript Author Manuscript

assisted laser desorption/ionization time of flight (MALDI-TOF) MS. Spectra were analyzed using Data Explorer Software (Applied Biosystems).

Cerebellar Cell Culture, Transfection and Electrophysiology—Primary cultures were prepared from WT mice as described previously (Linden, 1996). Cells were transfected by Helios Gene Gun System (Bio-Rad) and recorded as described previously (Smith-Hicks et al., 2010).

Mouse Strains—All mice in the study were in congenic C57BL/6J strain background and kept in standard housing with littermates with a 12:12 light-dark cycle. Free access to water and food were provided. All procedures involving animals were under the guidelines and supervision of JHMI Institutional Animal Care and Use Committee.

Generation of Arc$^{S260A/T278A}$ Knock-in Mice—Arc$^{S260A/T278A}$ knock-in mice were generated at the JHMI Transgenic Core Center. We used CCTop (CRISPR/Cas9 target online predictor, https://crispr.cos.uni-heidelberg.de/index.html) to search sgRNA sequence (5'-CTCCCGTGAAGCCATTCAGC-3') and to predict potential off-target sites. With the introduction of an oligonucleotide template, three point mutations were created: two of them caused the substitution of Serine 260 and Threonine 278 to Alanine, and the third mutation removed a PAM site in the oligonucleotide template and generated a synonymous mutation (no alteration of Arc protein sequence). The sequence of forward primer used for genotyping was 5'-GGTGGGTGGCTCTGAAGAAT-3', and the reverse primer was 5'-CCAGAGGAACTGGTCGAGTG-3' that generates a 220-bp PCR product. The identity of mice genotypes was confirmed by both sequencing and *BanII* (NEB R0119S) restriction-enzyme digestion that can recognize WT sequence but not the mutated S260A site. To screen the potential existence of off-target effect in our CRISPR-engineered mice, seven genes (*Ntrk3, Fhod3, Nisch, Sirpa, Spagl, Pent, Flnb*, and *Netl*) were selected for deep sequencing based on the predicted mutations in protein-coding region, critical for neuron growth and function, or on the same chromosome 15 as *Arc* locates.

Forebrain and P2 Fraction Lysate Preparation—8- to 9-week-old male mice were anesthetized with isoflourane upon disappearance of tail withdrawal reflex, followed by acute cervical dislocation. Mice were then decapitated, brain stem was removed, and the forebrain was obtained and immediately flash-frozen. During the lysate preparation, half of forebrain was lysed in 1.5 ml iced-cold pH 7.4 HEPES-buffered sucrose solution [0.32 M sucrose, 4 mM HEPES, 2 mM EDTA, 2 mM EGTA, with cOmplete protease and PhosSTop phosphatase inhibitors (Roche 11697498001 & 4906845001)] and homogenized with a motor driven glass-Teflon homogenizer at 800 rpm (20-25 strokes). To further prepare P2 fraction (crude synaptosomal membrane), forebrain homogenate was centrifuged at 800 × g at 4°C or 10 min to pellet down nuclear fraction (P1). The supernatant was spun at 10,000 × g at 4°C for 20 min to yield the pellet. The pellet was resuspended with HEPES-buffered sucrose solution and then respun at 10,000 ° g for another 20 min to yield the P2 crude synaptosomal fraction. The forebrain lysate and P2 fraction pellet were then mixed with SDS and Triton X-containing HEPES-buffered sucrose solution (with protease and phosphatase inhibitors), with the final concentration of 1% SDS and 1% Triton X-100. After

Author Manuscript Author Manuscript Author Manuscript Author Manuscript

sonication, samples were mixed constantly on a revolving mixer at 4°C for 60 min to ensure complete lysis. The concentration of protein was determined by BCA assay. Forebrain and P2 fraction lysates obtained from WT and $Arc^{S260A/T278A}$ knock-in mice were mixed with 2× Laemmli sample buffer (Biorad, 161-0737) for next step.

RNA Extraction, cDNA Synthesis, and Quantitative PCR—Half of forebrains from 8- to 9-week-old male WT and $Arc^{S260A/T278A}$ mice were collected and homogenized in 1 ml iced-cold TRIzol (ThermoFisher 15596026). After RNA was extract and purified, its concentration/purity was determined with Nanodrop and adjusted to 1 μg/μl with DEPC-H_2O. cDNA was then generated with SuperScript™ First-Strand Synthesis System for RT-PCR (ThermoFisher 11904018) using random hexamers. Quantitative PCR was performed with a StepOne Plus machine (Applied Biosystem) using PowerUp SYBR Green Master Mix (ThermoFisher A25780) in a 96-well optical plate. All reactions were run in triplicate. The experiment setting for qPCR cycling is 50 °C for 2 min, 95 °C for 10 min, and followed by 40 cycles of 95 °C for 15 sec, 60 °C for 30 sec and 72 °C for 30 sec. Cycle threshold (Ct) values were determined by the StepOne Plus software and adjusted manually. Primer3Plus software was used to design two sets of Arc primers that target the 5' and 3' region of Arc exon 1, respectively. Primers for GAPDH served as an internal control to normalize data.

Immunoblotting—10 μg protein of each sample was loaded onto 4%−12% NuPAGE Bis-Tris Gel with protein ladder and running with constant voltage of 130 V. After 3-hour transfer with constant 350 mA current, PVDF-membranes were blocked with 1% casein in 1× TBS (Biorad, 161-0782) for one hour at room temperature, and incubated overnight with primary antibodies at 4 °C (antibodies listed below). The incubation time for secondary antibody and antibody for loading control was 60 min at room temperature. Blots were imaged using either the Alphatek AX700 LE or the Biorad ChemiDoc MP Imaging System, depending on the secondary antibodies used.

Slice preparation and field potential recording—Hippocampal slices were prepared from 5-6 week-old Arc WT and homozygous $Arc^{S260A/T278A}$ mutant mice. Briefly, mice were anesthetized with the inhalation anesthetic isoflurane and decapitated. Horizontal 400 μm thick hippocampal slices were prepared with a vibratome (Leica VT1200S) in ice-cold oxygenated (95% O2 and 5% CO2) dissection solution containing (in mM): 75 NaCl, 26 NaHCO3, 75 sucrose, 25 glucose, 2.5 KC1, 1.25 NaH2PO4, 7 MgC12, and 0.5 CaC12. The area CA3 was removed to minimize recurrent activity. Slices were then gently transferred to a submersion chamber with oxygenated artificial cerebral spinal fluid (ACSF, 30 °C) containing (in mM): 124 NaCl, 26.2 NaHC03, 1.25 NaH2P04, 2.5 KC1, 20 glucose, 1.3 MgC12, 2.5 CaC12. After recovering for at least 2 hr, the hippocampal slices were transferred to submersion recording chamber (flow rate of ~3mL/min at 30 °C) for field potential recording. The field excitatory postsynaptic potentials (fEPSPs) were evoked every 30s with a parallel bipolar electrode (WPI, FL, USA) placed in the stratum radiatum of CA1, and recorded with a 1-2 MΩ glass recording electrode filled with ACSF (~200 μm away at orthodromic direction). Input-output curves were obtained for every slices and the baseline responses were set to yield ~40% max fEPSP for FTP experiments and ~55% max for LTD experiments. LTP was induced by theta burst stimulation: 4 trains of 10 bursts at 5 Hz with a

Author Manuscript Author Manuscript Author Manuscript Author Manuscript

10s inter-train interval, and each burst consisting of 4 stimuli given at 100 Hz. DHPG-LTD was induced with a 5 min long perfusion of 50 μM (S)-3,5-DHPG (Tocris, Bristol, UK).

Behavioral testing—All behavioral procedures involving animals were under the guidelines of JHU Institutional Animal Care and Use Committee. Behavioral testing was performed by personnel blind to genotype. Mice of both genotypes were littermate males and 3 months-old at the beginning of behavioral testing. During each behavioral test, mice were tracked and video-recorded by ANY-maze 6.0 software (Stoelting Co., Wood Dale, IL, US). Novelty-induced exploratory activation was analyzed in an open field arena (38 × 38 × 25 cm) during a 45-min session. Anxiety levels were assessed in the open field (by calculating thigmotaxis) and in a Plus maze (each arm 135 × 10 cm) (by calculating preferences to the open arms. Spatial memory was analyzed using Morris water maze (MWM) as described in (Chow et al., 2010). A reference memory version of the MWM that requires incremental learning of a constant platform location was conducted over three consecutive days. The start location for each trial was randomly predetermined. Two types of the probe trials were conducted daily. The short-delay probe trials were conducted 30 min after the last training trial, and the long-delay probe trials were conducted after an over-night delay (~20 hrs) and before the first training trial. Spatial preferences during the probe trials were calculated using time% spent in an area around the platform (a chance level 21%). Classical fear conditioning was conducted using Ugo Basile chambers (UgoBasile Inc., Italy) supported by Any-Maze software. During the training session (Session1), mice were habituated to the training context for 2 min, during which the level of “pretraining” freezing was measured. Then, a delayed conditioning paradigm was used consisting of three presentations of conditioned stimulus (CS: sound 600kHz, 15 sec duration, 85 dB intensity) co-terminated with an unconditioned stimulus (2 sec-long scrambled 0.4mA footshock). Inter-stimulus intervals (ITI) lasted 2 min and, after the 3rd presentation of CS-US pairing, mice remained in the context for additional 2 min to measure the final levels of freezing. Context- and Cue (Noise)-dependent fear behaviors were analyzed 24 (Session 2) and 28 (Session 3) hours later, respectively. The freezing behaviors were video-recorded and later analyzed by ANY-maze 6.0 software (Stoelting Co., Wood Dale, IL, US) using 2000ms/30on/40off thresholds for automatic freezing detection. Statistica 13.0 software (TIBCO Software Inc, Palo Alto, CA, US) was used for statistical analyses and visualization of data with minimal level of significance $P<0.05$ corrected by a Bonferroni-Holm test for multiple comparisons when appropriate. Data are presented as mean ± standard error of the mean (SEM) unless noted otherwise.

Supplementary Material

Refer to Web version on PubMed Central for supplementary material.

Acknowledgments

We thank Biogen for support during the initial studies and Jason Shepherd for helping to initiate electrophysiological studies. We are thankful to Tatiana Melnikova, Catherine LaCourse and Hye Won Chi for help in behavioral studies. Research support was provided by NARSAD (W.Z., P.F.W.), R01 NS095901 (D.J.L.), R01 MH053608 (D.J.L., P.F.W.), P50 MH100024 (D.J.L, R.L.H., P.F.W.).

Author Manuscript Author Manuscript Author Manuscript Author Manuscript

References

Ashley J, Cordy B, Lucia D, Fradkin LG, Budnik V, and Thomson T (2018). Retrovirus-like Gag Protein Arc1 Binds RNA and Traffics across Synaptic Boutons. Cell 172, 262–274 e211. [PubMed: 29328915]

Barklis E, Alfadhli A, McQuaw C, Yalamuri S, Still A, Barklis RL, Kukull B, and Lopez CS (2009). Characterization of the in vitro HIV-1 capsid assembly pathway. Journal of molecular biology 387, 376–389. [PubMed: 19356593]

Barylko B, Wilkerson JR, Cavalier SH, Binns DD, James NG, Jameson DM, Huber KM, and Albanesi JP (2018). Palmitoylation and Membrane Binding of Arc/Arg3.1: A Potential Role in Synaptic Depression. Biochemistry 57, 520–524. [PubMed: 29264923]

Byers CE, Barylko B, Ross JA, Southworth DR, James NG, Taylor C.A.t., Wang L, Collins KA, Estrada A, Waung M, et al. (2015). Enhancement of dynamin polymerization and GTPase activity by Arc/Arg3.1. Biochim Biophys Acta 1850, 1310–1318. [PubMed: 25783003]

Campillos M, Doerks T, Shah PK, and Bork P (2006). Computational characterization of multiple Gag-like human proteins. Trends Genet 22, 585–589. [PubMed: 16979784]

Chow VW, Savonenko AV, Melnikova T, Kim H, Price DL, Li T, and Wong PC (2010). Modeling an anti-amyloid combination therapy for Alzheimer's disease. Sci Transl Med 2, 13ra11.

Chowdhury S, Shepherd JD, Okuno H, Lyford G, Petralia RS, Plath N, Kuhl D, Huganir RL, and Worley PF (2006). Arc/Arg3.1 interacts with the endocytic machinery to regulate AMPA receptor trafficking. Neuron 52, 445–459. [PubMed: 17088211]

Cooper LN, and Bear MF (2012). The BCM theory of synapse modification at 30: interaction of theory with experiment. Nat Rev Neurosci 13, 798–810. [PubMed: 23080416]

El-Boustani S, Ip JPK, Breton-Provencher V, Knott GW, Okuno H, Bito H, and Sur M (2018). Locally coordinated synaptic plasticity of visual cortex neurons in vivo. Science 360, 1349–1354. [PubMed: 29930137]

Feng B, Raghavachari S, and Lisman J (2011). Quantitative estimates of the cytoplasmic, PSD, and NMDAR-bound pools of CaMKII in dendritic spines. Brain Res 1419, 46–52. [PubMed: 21925648]

Gewirtz JC, and Davis M (2000). Using pavlovian higher-order conditioning paradigms to investigate the neural substrates of emotional learning and memory. Learn Mem 7, 257–266. [PubMed: 11040256]

Goelet P, Castellucci VF, Schacher S, and Kandel ER (1986). The long and the short of longterm memory--a molecular framework. Nature 322, 419–422. [PubMed: 2874497]

Guzowski JF, McNaughton BL, Barnes CA, and Worley PF (1999). Environment-specific expression of the immediate-early gene Arc in hippocampal neuronal ensembles. Nature neuroscience 2, 1120–1124. [PubMed: 10570490]

Hell JW (2014). CaMKII: claiming center stage in postsynaptic function and organization. Neuron 81, 249–265. [PubMed: 24462093]

Helmstetter FJ, and Fanselow MS (1989). Differential second-order aversive conditioning using contextual stimuli. . Anim. Learn. Behav. 17, 205–212.

Jakkamsetti V, Tsai NP, Gross C, Molinaro G, Collins KA, Nicoletti F, Wang KH, Osten P, Bassell GJ, Gibson JR, et al. (2013). Experience-induced Arc/Arg3.1 primes CA1 pyramidal neurons for metabotropic glutamate receptor-dependent long-term synaptic depression. Neuron 80, 72–79. [PubMed: 24094104]

Kandel ER, Dudai Y, and Mayford MR (2014). The molecular and systems biology of memory. Cell 157, 163–186. [PubMed: 24679534]

Lawrence MC, and Colman PM (1993). Shape complementarity at protein/protein interfaces. Journal of molecular biology 234, 946–950. [PubMed: 8263940]

Linden DJ (1996). A protein synthesis-dependent late phase of cerebellar long-term depression. Neuron 17, 483–490. [PubMed: 8816711]

Linden DJ (2012). A late phase of LTD in cultured cerebellar Purkinje cells requires persistent dynamin-mediated endocytosis. J Neurophysiol 107, 448–454. [PubMed: 22049330]

Author Manuscript Author Manuscript Author Manuscript Author Manuscript

Lisman J, and Raghavachari S (2015). Biochemical principles underlying the stable maintenance of LTP by the CaMKII/NMDAR complex. Brain Res 1621, 51–61. [PubMed: 25511992]

McCurry CL, Shepherd JD, Tropea D, Wang KH, Bear MF, and Sur M (2010). Loss of Arc renders the visual cortex impervious to the effects of sensory experience or deprivation. Nature neuroscience 13, 450–457. [PubMed: 20228806]

Moorman S, Mello CV, and Bolhuis JJ (2011). From songs to synapses: molecular mechanisms of birdsong memory. Molecular mechanisms of auditory learning in songbirds involve immediate early genes, including zenk and arc, the ERK/MAPK pathway and synapsins. Bioessays 33, 377–385. [PubMed: 21381060]

Myers JB, Zaegel V, Coultrap SJ, Miller AP, Bayer KU, and Reichow SL (2017). The CaMKII holoenzyme structure in activation-competent conformations. Nat Commun 8, 15742. [PubMed: 28589927]

Myrum C, Baumann A, Bustad HJ, Flydal MI, Mariaule V, Alvira S, Cuellar J, Haavik J, Soule J, Valpuesta JM, et al. (2015). Arc is a flexible modular protein capable of reversible self-oligomerization. Biochem J 468, 145–158. [PubMed: 25748042]

Na Y, Park S, Lee C, Kim DK, Park JM, Sockanathan S, Huganir RL, and Worley PF (2016). Real-Time Imaging Reveals Properties of Glutamate-Induced Arc/Arg 3.1 Translation in Neuronal Dendrites. Neuron 91, 561–573. [PubMed: 27397520]

Niere F, Wilkerson JR, and Huber KM (2012). Evidence for a fragile X mental retardation protein-mediated translational switch in metabotropic glutamate receptor-triggered Arc translation and long-term depression. The Journal of neuroscience : the official journal of the Society for Neuroscience 32, 5924–5936. [PubMed: 22539853]

Okuno H, Akashi K, Ishii Y, Yagishita-Kyo N, Suzuki K, Nonaka M, Kawashima T, Fujii H, Takemoto-Kimura S, Abe M, et al. (2012). Inverse synaptic tagging of inactive synapses via dynamic interaction of Arc/Arg3.1 with CaMKIIbeta. Cell 149, 886–898. [PubMed: 22579289]

Otmakhov N, Regmi S, and Lisman JE (2015). Fast Decay of CaMKII FRET Sensor Signal in Spines after LTP Induction Is Not Due to Its Dephosphorylation. PLoS One 10, e0130457. [PubMed: 26086939]

Park S, Park JM, Kim S, Kim JA, Shepherd JD, Smith-Hicks CL, Chowdhury S, Kaufmann W, Kuhl D, Ryazanov AG, et al. (2008). Elongation factor 2 and fragile X mental retardation protein control the dynamic translation of Arc/Arg3.1 essential for mGluR-LTD. Neuron 59, 70–83. [PubMed: 18614030]

Pastuzyn ED, Day CE, Kearns RB, Kyrke-Smith M, Taibi AV, McCormick J, Yoder N, Belnap DM, Erlendsson S, Morado DR, et al. (2018). The Neuronal Gene Arc Encodes a Repurposed Retrotransposon Gag Protein that Mediates Intercellular RNA Transfer. Cell 172, 275–288 e218. [PubMed: 29328916]

Phillips RG, and LeDoux JE (1992). Differential contribution of amygdala and hippocampus to cued and contextual fear conditioning. Behav Neurosci 106, 274–285. [PubMed: 1590953]

Plath N, Ohana O, Dammermann B, Errington ML, Schmitz D, Gross C, Mao X, Engelsberg A, Mahlke C, Welzl H, et al. (2006). Arc/Arg3.1 is essential for the consolidation of synaptic plasticity and memories. Neuron 52, 437–444. [PubMed: 17088210]

Pornillos O, Ganser-Pornillos BK, Kelly BN, Hua Y, Whitby FG, Stout CD, Sundquist WI, Hill CP, and Yeager M (2009). X-ray structures of the hexameric building block of the HIV capsid. Cell 137, 1282–1292. [PubMed: 19523676]

Pornillos O, Ganser-Pornillos BK, and Yeager M (2011). Atomic-level modelling of the HIV capsid. Nature 469, 424–427. [PubMed: 21248851]

Rizley RC, and Rescorla RA (1972). Associations in second-order conditioning and sensory preconditioning. J Comp Physiol Psychol 81, 1–11. [PubMed: 4672573]

Rouvinski A, Guardado-Calvo P, Barba-Spaeth G, Duquerroy S, Vaney MC, Kikuti CM, Navarro Sanchez ME, Dejnirattisai W, Wongwiwat W, Haouz A, et al. (2015). Recognition determinants of broadly neutralizing human antibodies against dengue viruses. Nature 520, 109–113. [PubMed: 25581790]

Author Manuscript Author Manuscript Author Manuscript Author Manuscript

Schnabel R, Palmer MJ, Kilpatrick IC, and Collingridge GL (1999). A CaMKII inhibitor, KN-62, facilitates DHPG-induced LTD in the CA1 region of the hippocampus. Neuropharmacology 38, 605–608. [PubMed: 10221764]

Serriere J, Fenel D, Schoehn G, Gouet P, and Guillon C (2013). Biophysical characterization of the feline immunodeficiency virus p24 capsid protein conformation and in vitro capsid assembly. PLoS One 8, e56424. [PubMed: 23457565]

Shin SM, Zhang N, Hansen J, Gerges NZ, Pak DT, Sheng M, and Lee SH (2012). GKAP orchestrates activity-dependent postsynaptic protein remodeling and homeostatic scaling. Nature neuroscience 15, 1655–1666. [PubMed: 23143515]

Smith-Hicks C, Xiao B, Deng R, Ji Y, Zhao X, Shepherd JD, Posern G, Kuhl D, Huganir RL, Ginty DD, et al. (2010). SRF binding to SRE 6.9 in the Arc promoter is essential for LTD in cultured Purkinje cells. Nature neuroscience 13, 1082–1089. [PubMed: 20694003]

Sumioka A, Yan D, and Tomita S (2010). TARP phosphorylation regulates synaptic AMPA receptors through lipid bilayers. Neuron 66, 755–767. [PubMed: 20547132]

Tomita S, Stein V, Stocker TJ, Nicoll RA, and Bredt DS (2005). Bidirectional synaptic plasticity regulated by phosphorylation of stargazin-like TARPs. Neuron 45, 269–277. [PubMed: 15664178]

Volff JN (2009). Cellular genes derived from Gypsy/Ty3 retrotransposons in mammalian genomes. Ann N Y Acad Sci 1178, 233–243. [PubMed: 19845640]

Wall MJ, Collins DR, Chery SL, Allen ZD, Pastuzyn ED, George AJ, Nikolova VD, Moy SS, Philpot BD, Shepherd JD, et al. (2018). The Temporal Dynamics of Arc Expression Regulate Cognitive Flexibility. Neuron 98, 1124–1132 e1127. [PubMed: 29861284]

Wang YT, and Linden DJ (2000). Expression of cerebellar long-term depression requires postsynaptic clathrin-mediated endocytosis. Neuron 25, 635–647. [PubMed: 10774731]

Waung MW, Pfeiffer BE, Nosyreva ED, Ronesi JA, and Huber KM (2008). Rapid translation of Arc/Arg3.1 selectively mediates mGluR-dependent LTD through persistent increases in AMPAR endocytosis rate. Neuron 59, 84–97. [PubMed: 18614031]

Zhang W, Wu J, Ward MD, Yang S, Chuang YA, Xiao M, Li R, Leahy DJ, and Worley PF (2015). Structural basis of arc binding to synaptic proteins: implications for cognitive disease. Neuron 86, 490–500. [PubMed: 25864631]

Author Manuscript Author Manuscript Author Manuscript Author Manuscript

Highlights

1. Arc GAG domain is phosphorylated by CaMKII, which prevents Arc oligomerization.
2. Arc phosphorylation controls the magnitude of mGluR-dependent LTD.
3. Arc regulation by CaMKII phosphorylation is required for adaptive learning.

Author Manuscript Author Manuscript Author Manuscript Author Manuscript

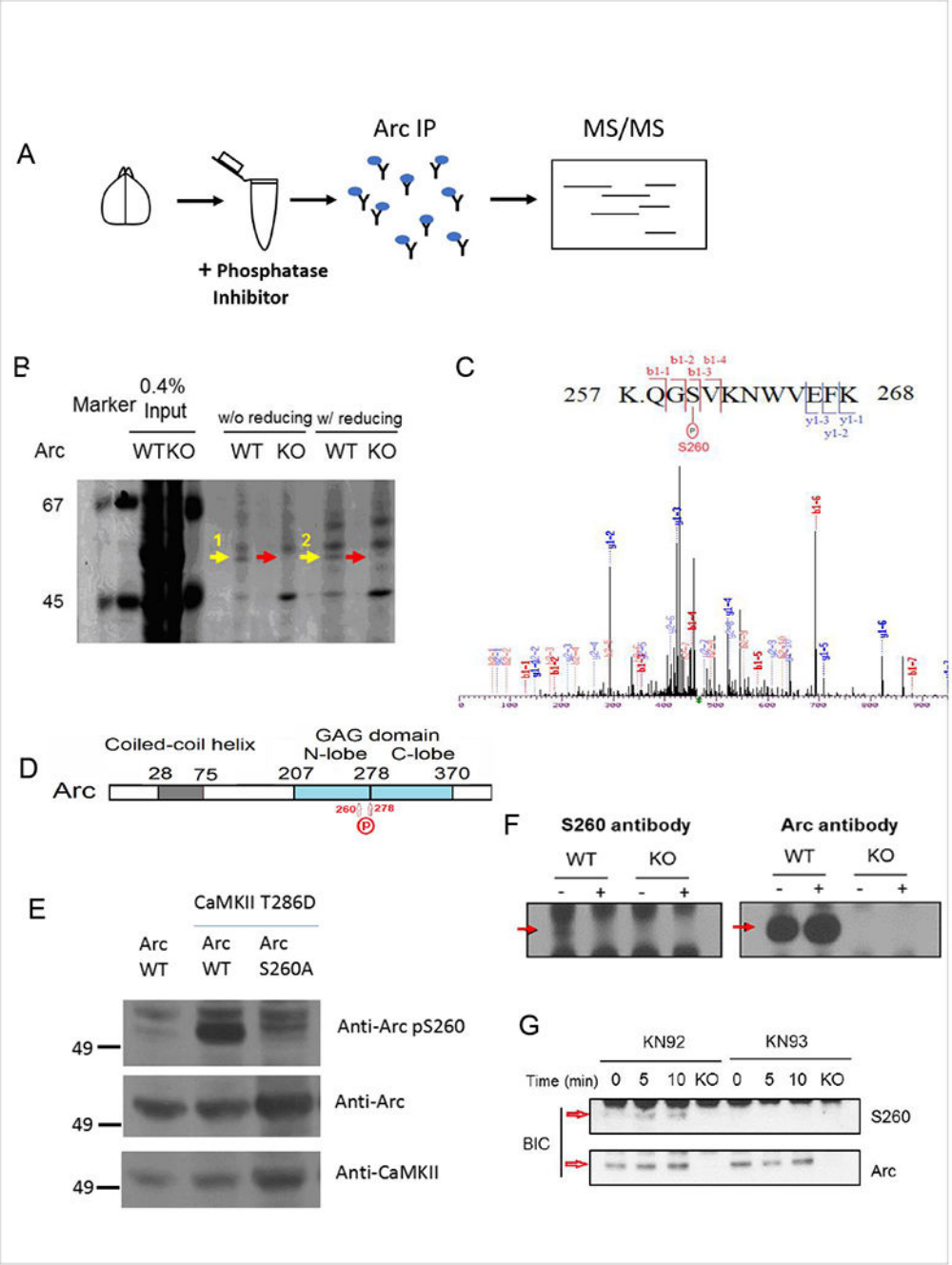

Figure 1. Identification of Arc phosphorylation sites

(A) Arc immunoprecipitation from naïve adult mouse brain and MS analysis. (**B)** Immunoprecipitates from detergent lysates of WT and Arc KO brain were sequentially eluted with 2% SDS and 2% SDS with 10 mM BME and analyzed by Coomassie. Arc band was excised and submitted for MS. Yellow arrows: Arc, Red arrows: Arc knockout control. (**C)** Mass spectrometry profile of the sequence of Arc from residues 257-268 is shown. Analysis by MS/MS revealed the presence of phosphorylated modification. The fragment ions whose m / z value corresponds to y or b ions (peptide fragments from C-terminus and

Author Manuscript Author Manuscript Author Manuscript Author Manuscript

from N-terminus, respectively) are indicated. The observed fragment ions are labeled on the spectrum and peptide sequence. (**D**) schematic of Arc indicating position of phosphorylation sites. (**E**) CaMKII phosphorylates ArcS260. Arc or ArcS260A were co-transfected with constitutively active CamKIIα (CamKII T286D) to HEK293 cells and cell lysates were blotted with ArcS260 phospho-specific antibody. (**F)** ArcS260 is phosphorylated in mouse brain. A parallel blot with Arc monoclonal antibody confirmed Arc immunoprecipitation and insensitivity to lambda phosphatase. (**G)** ArcS260 phosphorylation is induced in cultured neurons. Phospho-specific antibody revealed bicuculline-induced phosphorylation of ArcS260 that was blocked by 30 min pretreatment with CamKII inhibitor (KN93) but not control (KN92).

Author Manuscript Author Manuscript Author Manuscript Author Manuscript

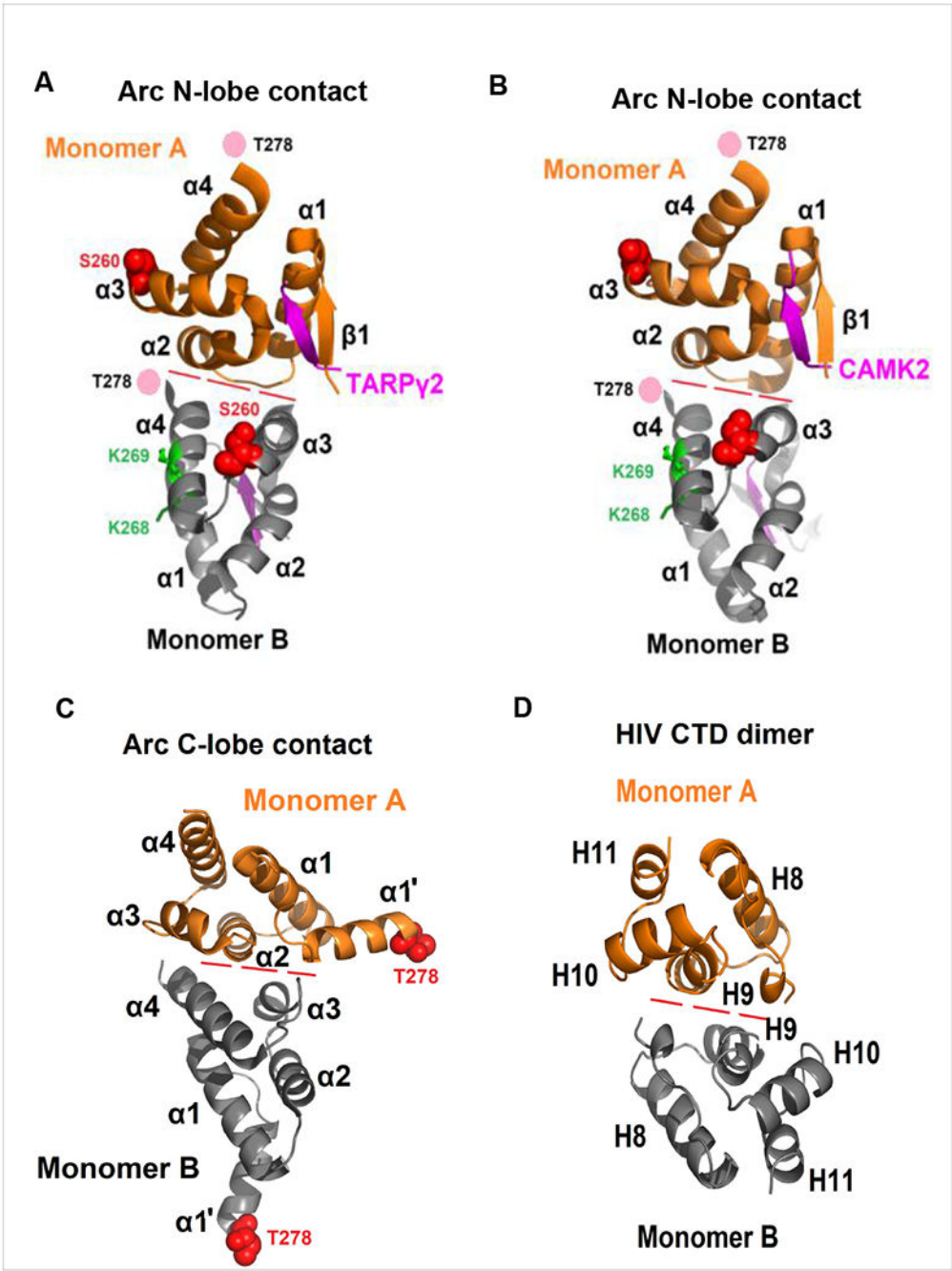

Figure 2. Comparison of dimers of Arc N-lobe, C-lobe and HIV C-lobe deduced from crystal structures.

Dimers are generated by application of crystal symmetry to the protomer present in the asymmetric unit. Red dashes indicate dimer interface of N-lobe or C-lobe. (**A, B**) Structures of complex crystals of Arc N-lobe with TARPγ2 peptide (PDB ID, 4X3H) or CamKII fragment (PDB ID, 4X3I). TARPγ2 peptide and CamKII fragment are colored purple. 260S is indicated in red ball. Unstructured 278T is displayed as a pink ball. Ubiquitination sites K268 and K269 are show in green. (**C**) Structure of Arc C-Lobe crystal (PDB ID, 4X3X).

278T is indicated in red ball. (**D**) HIV capsid CTD dimer (PDB ID, 1A43). In each case, the monomers that comprise the dimer are colored differently. Helix labels in parentheses follow references for Arc (Zhang et al., 2015) and HIV capsid domain (Pornillos et al., 2009).

Author Manuscript Author Manuscript Author Manuscript Author Manuscript

Author Manuscript Author Manuscript Author Manuscript Author Manuscript

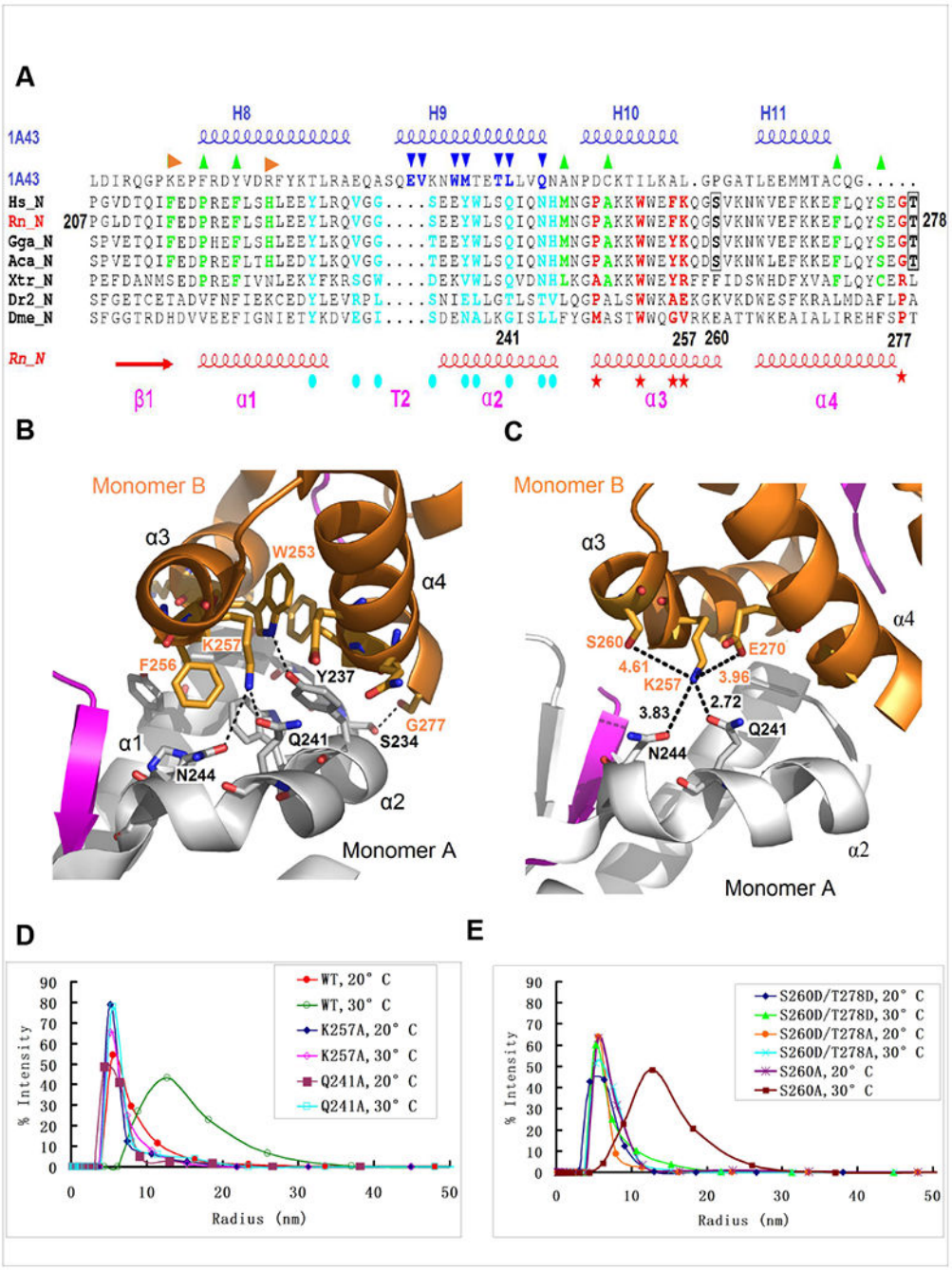

Figure 3. Arc N-lobe and oligomerization.

(**A**) The sequence alignment of Arc N-lobe (PDB ID, 4X3H) from typical species based on their 3D structural superposition with HIV capsid CTD (PDB ID, 1A43). Hs, *Homo sapiens*, NP_056008.1; Rn, *Rattus norvegicus*, NP_062234.1; Gga, *Gallus gallus*, NP_989763.1; Aca, *Anolis carolinensis*, XP_003223977.1; Xtr, *Xenopus (Silurana) tropicalis*, XP_002934511.1; Dme, *Drosophila melanogaster*, Arc1, Q7K1U0; Dr2, *Danio rerio*, XP_001919627; _N refer to N-lobe. Secondary structures of Arc N-lobe and HIV capsid CTD (PDB 1A43) are shown on the bottom in red and on the top in blue, respectively. The

Author Manuscript Author Manuscript Author Manuscript Author Manuscript

cyan solid circles (monomer A) and red stars (monomer B) below the sequence alignment mark amino acids that are predicted to mediate dimerization of Arc N-lobe. The green up triangles indicate hydrophobic pocket of Arc N-lobe, and the pair of aromatic residues supporting beta strand formation of N-lobe are highlighted with orange right deltoids. Blue down triangles indicate residues in the HIV C-lobe dimer interface. The phosphorylation sites S260 and T278 are shown in bold black with box. (**B-C**) magnified view of the interaction between two subunits of Arc N-lobe in grey (monomer A) and brown (monomer B), separately (PDB ID, 4X3H). The residues important for interaction are shown as a stick representation. (**D-E**) Polymerization status of various full-length Arc proteins in solution (10uM) examined by dynamic light scattering (DLS) with increasing temperature (1°C/min) from 20°C to 30°C and assayed after an additional 20 min at 30°C. (**D**) Mutation of predicted dimerization sites prevents oligomerization. (**E**) Phosphomimic mutations of S260 prevent oligomerization.

Author Manuscript Author Manuscript Author Manuscript Author Manuscript

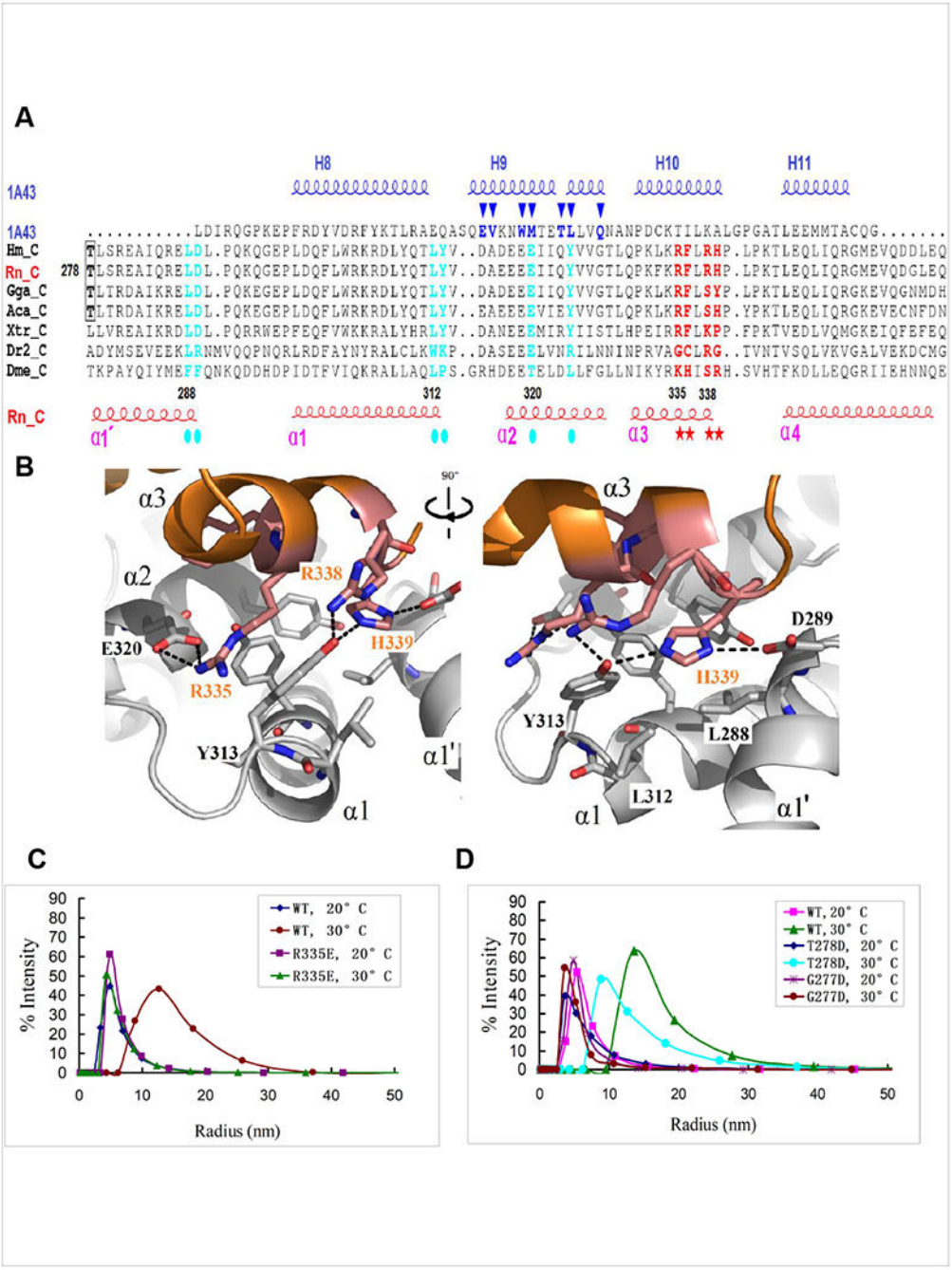

Figure 4. Arc C-Lobe and oligomerization.

(**A**) The sequence alignment of Arc C-lobe (PDB ID, 4X3X) for typical species based on their 3D structural superposition with HIV capsid CTD (PDB ID, 1A43). Hs, *Homo sapiens*, NP_056008.1; Rn, *Rattus norvegicus*, NP_062234.1; Gga, *Gallus gallus*, NP_989763.1; Aca, *Anolis carolinensis*, XP_003223977.1; Xtr, *Xenopus (Silurana) tropicalis*, XP_002934511.1; Dme, *Drosophila melanogaster*, Arcl, Q7K1U0; Dr2, *Danio rerio*, XP_001919627; _C refer to C-lobe. Secondary structures of Arc C-lobe and HIV capsid CTD (PDB 1A43) are shown on the bottom in red and on the top in blue, respectively. The

Author Manuscript Author Manuscript Author Manuscript Author Manuscript

cyan solid circles (monomer A) and red stars (monomer B) below the sequence alignment mark amino acids that mediate inter-subunit interactions of Arc C-lobe. The blue down triangles indicate residues in the HIV C-lobe dimer interface. The phosphorylation site T278 is shown in bold black with box. (**B**) Detailed view of the interaction between two subunits of Arc C-lobe in grey (monomer A) and brown (monomer B), separately (PDB ID, 4X3X). The residues important for interaction are shown as a stick representation. (**C, D**) Polymerization status of various full-length Arc proteins examined in solution (10uM) with increasing temperature (1°C/min) from 20°C to 30°C. (**C**) Mutations in the putative hinge region. After an additional 6 minutes at 30°C the mutant ArcT278D peaks ~1276 KDa (hexamer of tetramers) calculated based on gyration radius, while WT Arc peaks ~2458 KDa (dodecamer of tetramers). (**D**) Mutation of the C-lobe interface blocks oligomerization of full-length Arc.

Author Manuscript
Author Manuscript
Author Manuscript
Author Manuscript

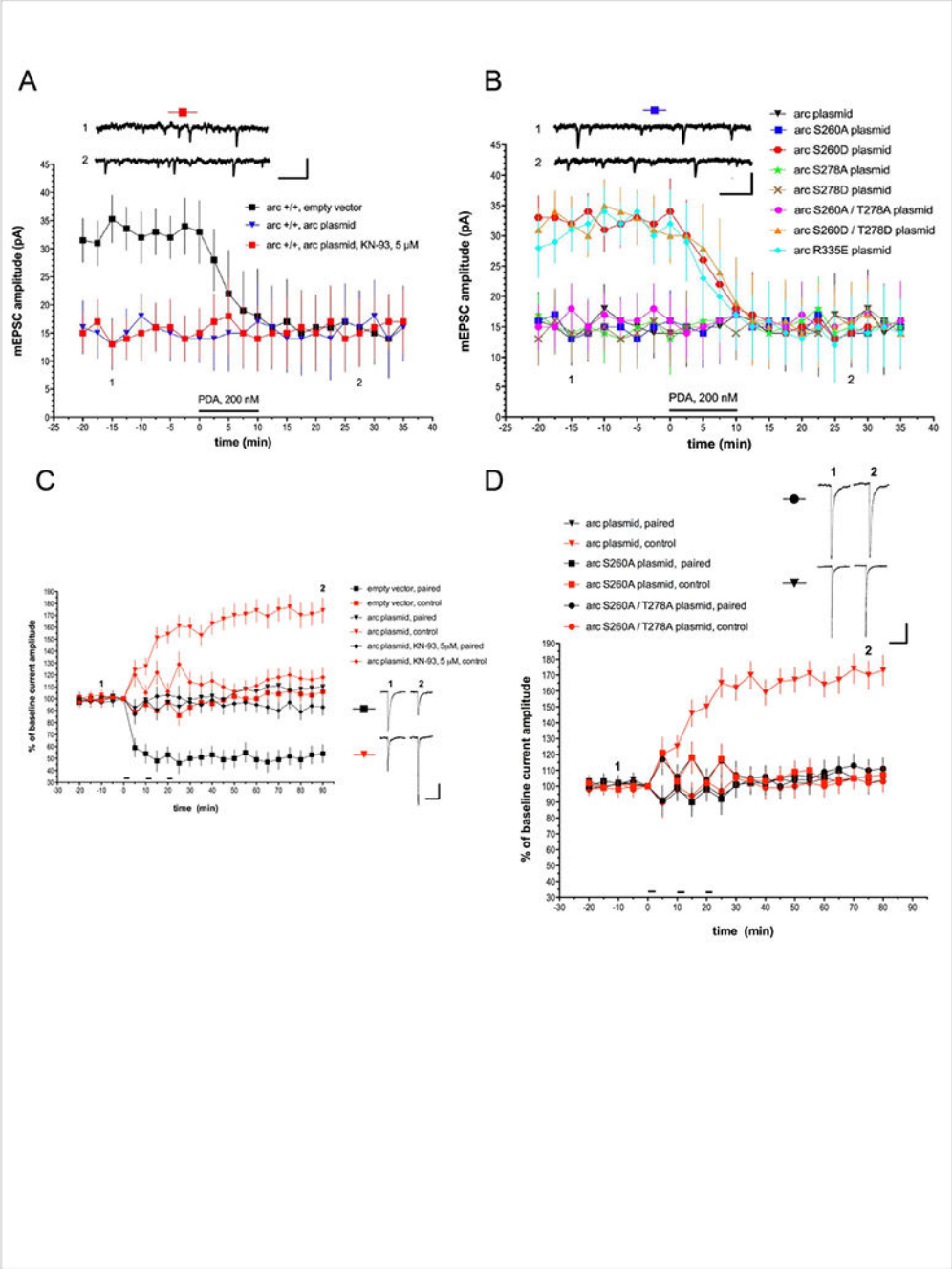

Figure 5. Arc oligomerization, synaptic function and regulation by CaMKII.

Whole-cell voltage-clamp recordings from mouse Purkinje cells expressing Arc transgenes in culture. (**A**) Basal mEPSC amplitude was driven low and chemical LTD evoked by PDA was occluded in Arc-transfected Purkinje cells. This effect was not blocked by pretreatment with the CaMKII inhibitor KN-93. N= 10 cells/group. (**B**) Phosphomimic mutant at the site S260 and C-lobe mutant R335E did not reduce the basal amplitude of mEPSCs and did not occlude subsequent PDA-evoked chemical LTD. ArcS260A mimics WT Arc by reducing mEPSC and occluding chemical LTD. N= 10 cells/group. The scale bars for the insets on

Author Manuscript Author Manuscript Author Manuscript Author Manuscript

(A) and (B) are both 500 msec, 20 pA. (**C**) Purkinje cells in primary cerebellar culture were transfected with Arc transgene or an empty vector control plasmid and examined using a standard protocol that induces dendrite-specific LTD in Purkinje cells treated with the control plasmid (n=8; or untransfected cells, not shown). In Arc expressing cells (n=7) LTD was occluded in the paired pathway that received glutamate/depolarization conjunction as indicated by the horizontal bars (paired pathway), while LTP was induced in the control pathway. LTP was abolished by pretreatment with the CamKII inhibitor KN-93 (n=8). Scale bars = 2 sec, 50 pA. (**D**) LTD induced by glutamate/depolarizing pairing (indicated by horizontal bars) was occluded by both WT, ArcS260A and ArcS260,T278A. LTP of control pathway was abolished in neurons expressing de-phosphorylation mimic mutants at ArcS260A. Arc plasmid (n=7); Arc S260A plasmid (n=8); Arc S260A,T278A plasmid (n=6). Scale bars = 2 sec, 60 pA.

Author Manuscript Author Manuscript Author Manuscript Author Manuscript

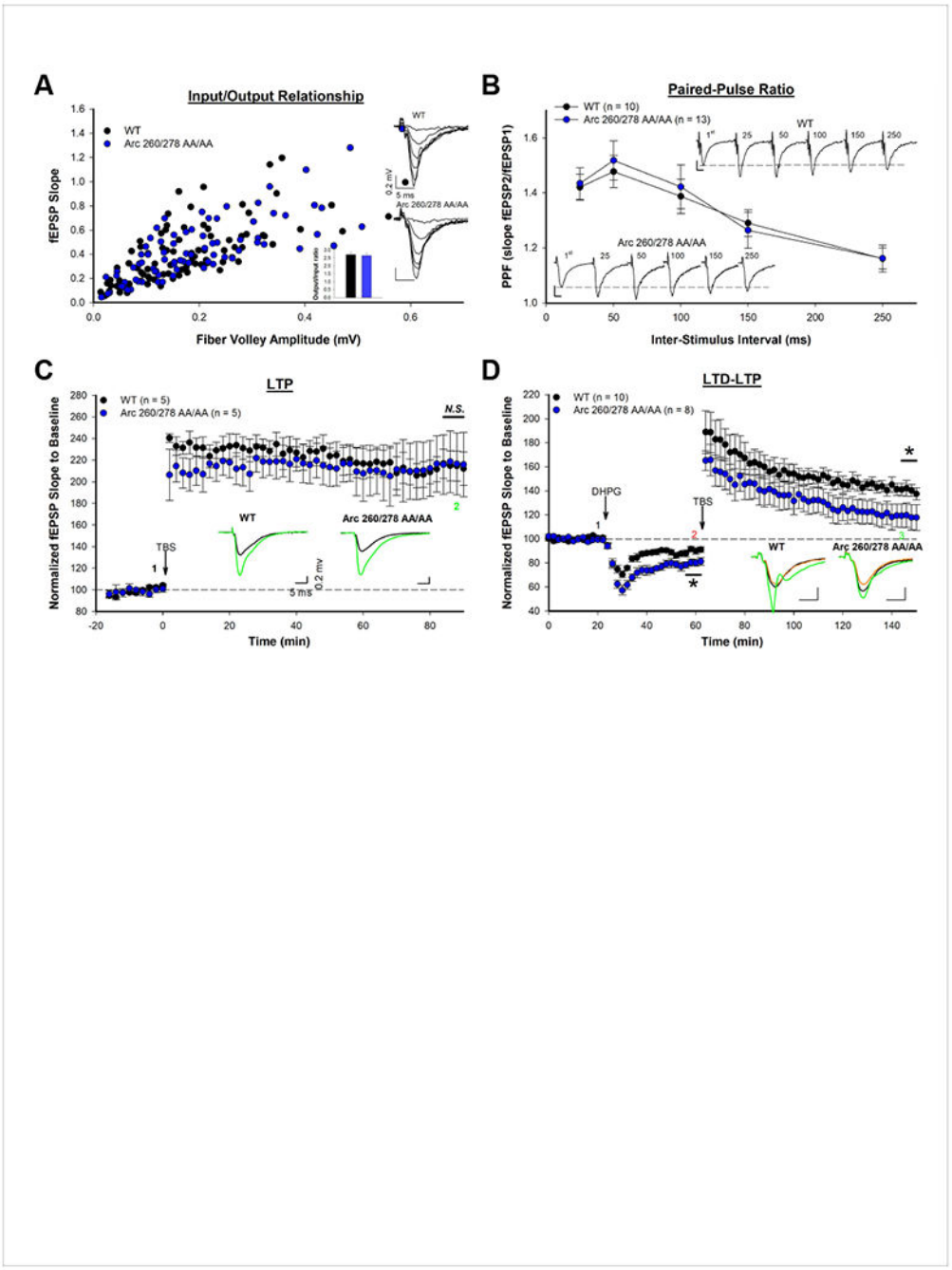

Figure 6. Enhanced DHPG-induced LTD in Arc 260/278 AA/AA mutant mice.

(A) The input-output ratio is not altered in Arc 260/278 AA/AA mutant mice. For input-output ratio: WT n = 86, I/O =2.70 ± 0.15 ms^{-1}; Mutant n=81, I/O = 2.64 ± 0.14 ms^{-1}. P>0.05 with two-tailed student's *t*-test. **(B)** Paired pulse facilitation is not altered in Arc 260/278 AA/AA mutant mice. WT n=13; Mutant n = 10. P>0.05 with two-way repeated measures ANOVA with Bonferoni post-hoc test. (**C**) Theta-burst stimulation (TBS) induced LTP is not altered in Arc 260/278 AA/AA mutant mice. n=5 for each group. P>0.05 with two-tailed student's *t*-test. (D) DHPG-induced LTD is significantly enhanced in Arc 260/278

Author Manuscript Author Manuscript Author Manuscript Author Manuscript

AA/AA mutant mice. The TBS-induced LTP following DHPG-LTD is significantly reduced in Arc 260/278 AA/AA mutant mice when normalized to original baseline, but not to last 6 min of LTD (see supplement figure S5). WT n=10; mutant n=8. * $P<0.05$ with two-tailed student's *t*-test.

Author Manuscript Author Manuscript Author Manuscript Author Manuscript

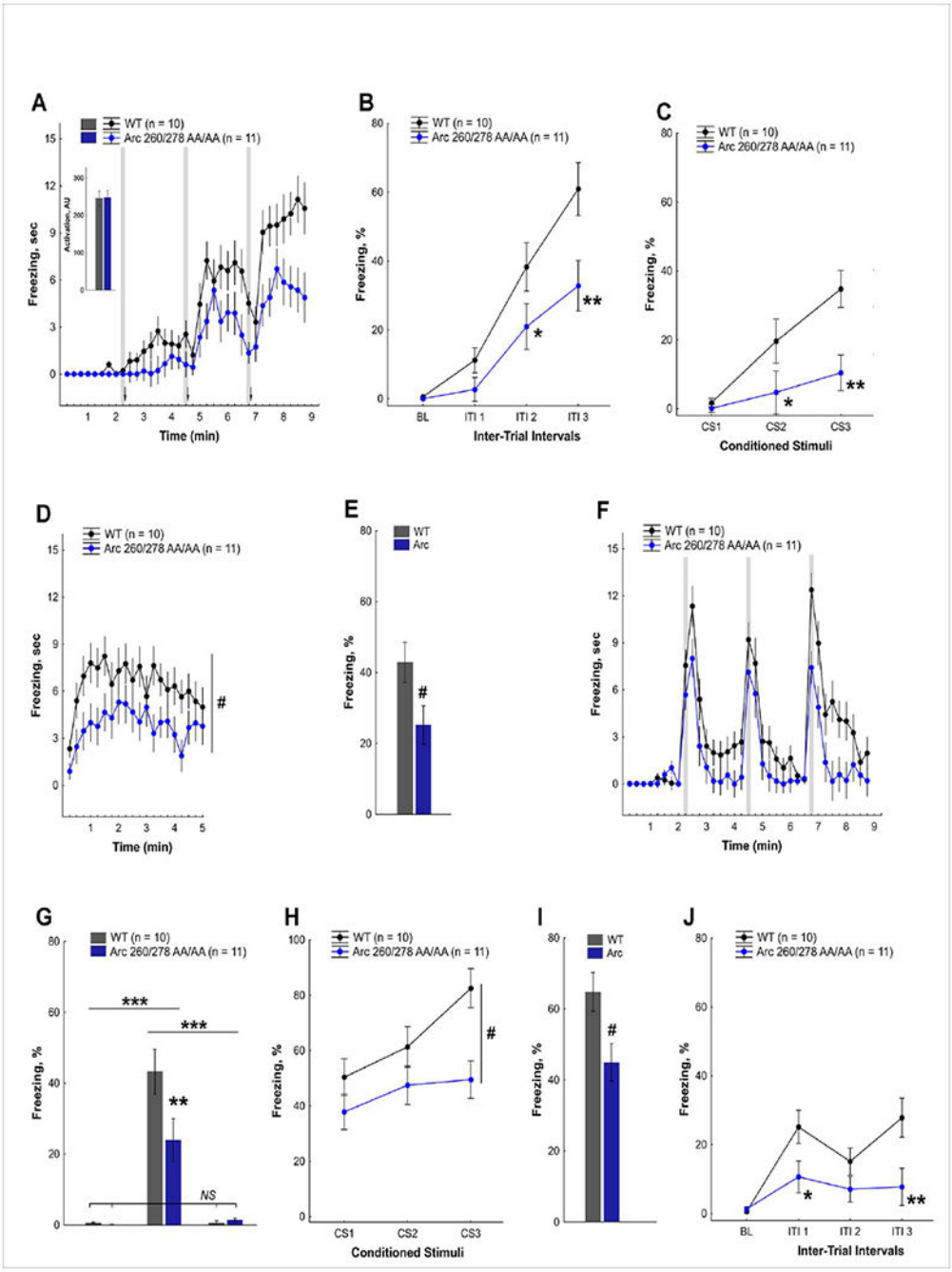

Figure 7. Arc 260/278 AA/AA mutant mice are deficient in acquisition of fear memory.

(A) Time course of freezing to context and conditioned stimulus, CS (shaded areas), observed in Arc 260/278 AA/AA mutant mice and littermate control WT mice during training in a delayed fear conditioning (Session 1). Arrows indicate presentation of unconditioned stimulus, US (a foot-shock) at the end of each CS. Insert shows equal sensitivity to a foot-shock in both genotypes (ANOVA, $F(1, 19)=0.1$, $P>0.9$). (**B**) Acquisition of fear to context is delayed in Arc 260/278 AA/AA mice (ANOVA, effect of genotype $F(1,19)=5.63$, $P<0.028$; genotype × intertrial interval (ITI) interaction $F(3,57)=4.23$,

Author Manuscript Author Manuscript Author Manuscript Author Manuscript

P<0.009). Pre-training basal levels (BL) of freezing were low in both genotypes. (**C**) Acquisition of fear to a conditioned stimulus (CS) is impaired in Arc 260/278 AA/AA mice (ANOVA, effect of genotype F(1,19)=7.60, P<0.013; genotype × inter-trial interval (ITI) interaction F(2,38)=3.98, P<0.027). (**D**) Time course of freezing to the training context after a 24-hr delay (Session 2). (**E**) Long-term contextual fear memory was impaired in Arc 260/278 AA/AA mice (ANOVA, effect of genotype F(1,19)=5.05, P<0.037; genotype × time block interaction, P>0.7). Average levels of freezing in Session 2 are shown. (**F**) Time course of freezing after a 28-hr delay tested in a new context before and after presentation of the CS (shown as shaded areas) (Session 3). (**G**) Freezing (time %) in the 1st 2 min of each session (S1, S2, S3) indicated no generalization of fear to a new context in either genotype. Initial levels of freezing in Session1 and Session 3 were comparable (P>0.8, NS) but dramatically lower than in Session 2 (ANOVA, effect of genotype F(1,19)=4.29, P<0.052, genotype × session interaction F(2,38)=5.22), P<0.009). (**H**) Long-term fear memory to the CS was impaired in Arc 260/278 AA/AA mice (ANOVA, effect of genotype F(1,19)=6.77, P<0.018; genotype × inter-trial interval (ITI) interaction, P>0.11). (**I**) Average levels of freezing to the CS were lower in Arc 260/278 AA/AA mice than in their WT littermates. (**J**) Acquisition of secondary fear to the new context was impaired in Arc 260/278 AA/AA mice (ANOVA, effect of genotype F(1,19)=5.34, P<0.032, genotype × session interaction F(3,57)=4.49), P<0.007). ITI - intertrial intervals in Session 3. Single and double asterisks in panels **B-C, G**, and **J** indicate significant deficits in Arc 260/278 AA/AA mice at p levels 0.05 (*) or 0.001 (**) (LSD post-hoc tests applied to a significant interaction in ANOVA). Pound signs in panels D-E and H-J indicate significant differences between genotypes (ANOVA, main effect of genotype, P<0.05). Numbers of cases are shown next to the labels.

Author Manuscript Author Manuscript Author Manuscript Author Manuscript

KEY RESOURCES TABLE

REAGENT or RESOURCE	SOURCE	IDENTIFIER
Antibodies		
Chicken anti-GFP polyclonal antibody	Thermo Fisher	Cat# A10262, RRID:AB_2534023
Mouse anti-HA monoclonal antibody	Sigma	Cat# H3663, RRID:AB_262051
Rabbit anti-Arc polyclonal anitbody	Zhang et al., 2015	N/A
Mouse anti-Arc monoclonal anitbody	Zhang et al., 2015	N/A
Goat anti-chicken Alexa-488 antibody	Thermo Fisher	Cat# A-11039, RRID:AB_2534096
Goat anti-mouse Alexa-633 antibody	Thermo Fisher	Cat# A-21052, RRID:AB_2535719
Goat anti-rabbit Alexa-555 antibody	Thermo Fisher	Cat# A32732, RRID:AB_2633281
Rabbit Anti-GluR1 Monoclonal Antibody	Millipore	Cat#04-855; RRID:AB_1977216
Anti-Ionotropic Glutamate receptor 2 antibody	Abcam	Cat#ab133477; RRID:AB_2620181
Mouse Anti-mGluR1 Monoclonal Antibody	BD Biosciences	Cat#610965; RRID:AB_398278
Rabbit Anti-mGluR5 Monoclonal Antibody	Abcam	Cat#2237-1; RRID:AB_1267242
PSD95 Antibody	Thermo Fisher Scientific	Cat#MA1-046; RRID:AB_2092361
Rabbit Anti-Stargazin Polyclonal antibody	Millipore	Cat#07-577; RRID:AB_310726
Sheep Anti-Mouse IgG - Horseradish Peroxidase antibody	GE Healthcare	Cat#NA931; RRID:AB_772210
StarBright™ Blue 700 Goat Anti-Mouse IgG	Bio-Rad	Cat#12004159
Donkey Anti-Rabbit IgG, Whole Ab ECL Antibody, HRP Conjugated	GE Healthcare	Cat#NA934; RRID:AB_772206
StarBright™ Blue 700 Goat Anti-Rabbit IgG	Bio-Rad	Cat#12004162
hFAB™ Rhodamine Anti-Tubulin Primary Antibody	Bio-Rad	Cat#12004165
CaMKII (pan) Antibody	Cell Signaling Technology	Cat# 3362; RRID:AB_2067938
Rabbit Anti-GluR3 Monoclonal Antibody	Abcam	Cat# ab40845; RRID:AB_776310
Bacterial and Virus Strains		
E.Coli DH5 alpha	Lab strain	N/A
E.Coli Rosetta (DE3)	Novagen	Cat #70954
E.Coli BL21 (DE3)	NEB	Cat #C2527
Chemicals, Peptides, and Recombinant Proteins		
Arc T278 phosphorylation peptide pT278-QYSEG{PTHR}LSRE	AnaSpec Inc.	N/A
(S)-3,5-DHPG	Tocris, Bristol, UK	Cat #0805
Arc S260 phosphorylation peptide pS260-EFKQG{PSER}VKNW	AnaSpec Inc.	N/A
Critical Commercial Assays		
QuickChange II Site-Directed Mutagenesis Kit	Agilent	Cat # 200524
Deposited Data		
Raw Data	Mendeley	http://dx.doi.org/10.17632/tt3hrs3r2m.1
Experimental Models: Cell Lines		
HEK293T	ATCC	ATCC#CRL-11268
Experimental Models: Organisms/Strains		

Author Manuscript Author Manuscript Author Manuscript Author Manuscript

REAGENT or RESOURCE	SOURCE	IDENTIFIER
Mouse: C57BL/6J $Arc^{S260A/T278A}$ knock-in	This paper	N/A
Oligonucleotides		
Mouse Arc, set 1 Forward primer 5'-GGCATCTGTTGACCGAAGTG-3'	This paper	N/A
Mouse Arc, set 1 Reverse primer 5'-GGCCTTGATGGACTTCTTCC-3'	This paper	N/A
Mouse Arc, set 2 Forward primer 5'-TGGAGCAGCTTATCCAGAGG-3'	This paper	N/A
Mouse Arc, set 2 Reverse primer 5'-TATTCAGGCTGGGTCCTGTC-3'	This paper	N/A
Mouse GAPDH Forward primer 5'-AGAAGGCTGGGGCTCATTTG-3'	This paper	N/A
Mouse GAPDH Reverse primer 5'-AGGGGCCATCCACAGTCTTC-3'	This paper	N/A
Mouse Arc genotyping Forward primer 5'-GGTGGGTGGCTCTGAAGAAT-3'	This paper	N/A
Mouse Arc genotyping Reverse primer 5'-CCAGAGGAACTGGTCGAGTG-3'	This paper	N/A
Recombinant DNA		
pGEX6P-full lenght Arc	This paper	N/A
pGEX6P-Stargazin(203-323)	Zhang et al., 2015	N/A
pGEX6P-Arc(207-370)	Zhang et al., 2015	N/A
pRK5-Arc	This paper	N/A
pRK5-HA-Endophilin3	This paper	N/A
GFP-RAB5	Kind Gift of Mike Ehlers	N/A
GFP-RAB7	Kind Gift of Mike Ehlers	N/A
GFP-RAB11	Kind Gift of Mike Ehlers	N/A
pRK5-myc-CAMK2A-T286D	Kind Gift of Richard Huganir	N/A
Software and Algorithms		
Dynamics™ v.6 software	Wyatt Technology	N/A
Data Explorer Software	Applied Biosystems	N/A
ANY-maze 6.0 software	Stoelting Co., Wood Dale, IL, US	N/A
Statistica 13.0 software	TIBCO Software Inc, Palo Alto, CA, US	N/A
GraphPad Prism version 5.0	GraphPad Software, San Diego, CA	N/A
Pymol	Schrödinger, LLC.	N/A
Other		
PhosSTOP	Roche	Cat #4906845001
Protease Inhibitors Cocktail Tablets	Roche	Cat #11836170001